The Astrophysical Journal, 645:613–633, 2006 July 1

NEAR-ULTRAVIOLET OBSERVATIONS OF HD 221170: NEW INSIGHTS INTO THE NATURE OF *r*-PROCESS–RICH STARS[1]

Inese I. Ivans,[2,3,4] Jennifer Simmerer,[5] Christopher Sneden,[5] James E. Lawler,[6]
John J. Cowan,[7] Roberto Gallino,[8,9] and Sara Bisterzo[8]

Received 2005 October 21; accepted 2006 February 17

ABSTRACT

Employing high-resolution spectra obtained with the near-UV–sensitive detector on the Keck I HIRES, supplemented by data obtained with the McDonald Observatory 2d-coudé, we have performed a comprehensive chemical composition analysis of the bright *r*-process–rich metal-poor red giant star HD 221170. Analysis of 57 individual neutral and ionized species yielded abundances for a total of 46 elements and significant upper limits for an additional five. Model stellar atmosphere parameters were derived with the aid of ~200 Fe peak transitions. From more than 350 transitions of 35 neutron-capture ($Z > 30$) species, abundances for 30 neutron-capture elements and upper limits for three others were derived. Utilizing 36 transitions of La, 16 of Eu, and seven of Th, we derive ratios of $\log \epsilon(\mathrm{Th/La}) = -0.73$ ($\sigma = 0.06$) and $\log \epsilon(\mathrm{Th/Eu}) = -0.60$ ($\sigma = 0.05$), values in excellent agreement with those previously derived for other *r*-process–rich metal-poor stars such as CS 22892−052, BD +17 3248, and HD 115444. Based on the Th/Eu chronometer, the inferred age is 11.7 ± 2.8 Gyr. The abundance distribution of the heavier neutron-capture elements ($Z \geq 56$) is fitted well by the predicted scaled solar system *r*-process abundances, as also seen in other *r*-process–rich stars. Unlike other *r*-process–rich stars, however, we find that the abundances of the lighter neutron-capture elements ($37 < Z < 56$) in HD 221170 are also in agreement with the abundances predicted for the scaled solar *r*-process pattern.

Subject headings: Galaxy: abundances — Galaxy: evolution — nuclear reactions, nucleosynthesis, abundances — stars: abundances — stars: individual (HD 221170) — stars: Population II

Online material: machine-readable tables

1. INTRODUCTION

The bulk of the neutron-capture (*n*-capture) elements beyond the iron group are created by some combination of the slow and rapid *n*-capture nucleosynthesis processes (*s*- and *r*-process), with each responsible for approximately half of the isotopes. In the *r*-process, both the neutron density and neutron flux are high. Neutron-rich sites associated with massive-star core-collapse supernovae (SNe II) are the likeliest sites for the *r*-process (see, e.g., Cowan & Thielemann 2004 and references therein), although the astrophysical site of the *r*-process has yet to be identified. Possible sites for the *r*-process include SN winds/hot bubbles (see, e.g., Hoffman et al. 1997; Terasawa et al. 2002; Wanajo et al. 2002; Kohri et al. 2005 and references therein), disks and jets (e.g., Cameron 2003 and references therein), neutron star mergers (e.g., Freiburghaus et al. 1999; Rosswog et al. 1999 and references therein; but for a contrasting view see Argast et al. 2004), and/or neutron star formation during accretion-induced collapse (e.g., Wheeler et al. 1998; Cohen et al. 2003; Qian & Wasserburg 2003).

Among the isotopes formed in the *r*-process are the radioactive group of elements known as the actinides, which include isotopes of Th and U. Due to their known radioactive decay rates, the abundances of Th (and U) in low-metallicity stars have been employed to derive the ages of presumably some of the oldest stars in the Galaxy, thereby setting a minimum for the age of the universe. Critical assumptions in the analysis of the observations are that the production ratios of the elements are known and that the elements under investigation arise from the same nucleosynthetic site. Following earlier work on the derivation of Th abundances and/or Th-based ages by Butcher (1987), Pagel (1989), and François et al. (1993), Sneden et al. (1996) derived the first Th/Eu-based nucleocosmochronometric age for a very metal-poor star: CS 22892−052, whose extreme *r*-process abundance enhancements were discovered by McWilliam et al. (1995). This was followed soon after by other Th/Eu-based age determinations of very metal-poor stars by Pfeiffer et al. (1997), Cowan et al. (1999, 2002), Sneden et al. (2000b), Johnson & Bolte (2001), and Hill et al. (2002). In most of these studies, the use of Th/Eu cosmochronometry has yielded consistent results (e.g., CS 22892−052, HD 115444, and BD +17 3248).

A weak U detection was made in BD +17 3248 (Cowan et al. 2002), and an upper limit was derived for CS 22892−052 (Sneden et al. 2000a, 2003), permitting lower limits to be placed on ages inferred by the Th/U ratio, which turn out to be in accord with those derived from Th/Eu cosmochronology. However, in the case of CS 31082−001, for which the first U abundance determination was made in an ultra–metal-poor star (Cayrel et al. 2001), the age

[1] Some of the data presented herein were obtained at the W. M. Keck Observatory, which is operated as a scientific partnership among the California Institute of Technology, University of California, and NASA and was made possible by the financial support of the W. M. Keck Foundation. This paper includes data taken at the McDonald Observatory of the University of Texas at Austin.

[2] Observatories of the Carnegie Institution of Washington, 813 Santa Barbara Street, Pasadena, CA 91101; iii@ociw.edu.

[3] Princeton University Observatory, Peyton Hall, Princeton, NJ 08544.

[4] Carnegie-Princeton Fellow.

[5] Department of Astronomy, University of Texas, RLM 15.308, Austin, TX 78712; jensim@astro.as.utexas.edu, chris@verdi.as.utexas.edu.

[6] Department of Physics, University of Wisconsin, 1150 University Avenue, Madison, WI 53706; jelawler@wisc.edu.

[7] Homer L. Dodge Department of Physics and Astronomy, University of Oklahoma, Room 131 Nielsen Hall, Norman, OK 73019; cowan@nhn.ou.edu.

[8] Dipartimento di Fisica Generale, Università di Torino, Via P. Giuria 1, 10125 Torino, Italy; gallino@ph.unito.it, bisterzo@ph.unito.it.

[9] Centre for Stellar and Planetary Astrophysics, School of Mathematical Sciences, Building 28, Monash University, Victoria 3800, Australia.

inferred from Th/Eu is found to be significantly different from that inferred from Th/U (Hill et al. 2002). Discrepant age results have also been reported for HD 221170 by Yushchenko et al. (2005) employing the abundances they derived for Th/U and Th/Eu.

The fundamental assumption built into the technique of applying these abundances to derive ages via nucleocosmochemistry is that the elements are created in the same processes, i.e., the same nucleosynthetic sites, and track the contributions of that process through Galactic chemical evolution; i.e., a production ratio can be specified. There is no doubt that all of the Th and U is produced in the *r*-process: the termination point of the *s*-process occurs at ^{209}Bi. Isotopes heavier than ^{209}Bi decay too quickly to be built by the *s*-process. In addition, Eu is predominantly an *r*-process element: roughly 90% of the solar Eu was produced this way (Käppeler et al. 1989; Arlandini et al. 1999; Burris et al. 2000; Simmerer et al. 2004; Travaglio et al. 2004). However, Th lies 29 amu away from Eu. It has been argued that the production of the actinide elements may not be known sufficiently well to trust their use as nucleocosmochronometers (see, e.g., Arnould & Goriely 2001 and references therein). Certainly, with lighter *n*-capture isotopes, there is evidence that multiple *r*-process sites or sources have contributed to the total abundance in both the Sun and metal-poor stars. While at low metallicities the observed abundances of *r*-process–rich stars in the atomic range of $Z \geq 56$ are in good agreement with the predicted scaled solar *r*-process patterns (Sneden et al. 1996, 1998; Cowan et al. 1999), the abundances of the lighter *n*-capture elements are not (Sneden et al. 2000a). Furthermore, based on studies of the inferred abundances of short-lived isotopes in the early solar system, multiple sites or sources have been required to explain the early solar system abundances of both light and heavy isotopes normally considered to be of primary *r*-process origin (see, e.g., Cameron et al. 1993; Wasserburg et al. 1996; Meyer & Clayton 2000).

In the Sun, the abundances are the integrated result of many generations of stars, including millions of SNe II, and depend on the details of the star formation history, initial mass function, chemical yields, etc. However, the heavy-element abundances most useful for unravelling the origins of the *r*-process correspond to those observed in stars that formed from material with little prior nucleosynthetic processing, such as the relatively pristine material out of which extremely metal-poor stars were born. To further explore the *n*-capture elemental abundances in *r*-process–rich stars, we observed the bright ($V = 7.7$) metal-poor red giant branch star HD 221170.

HD 221170 has been the subject of over 40 years of spectroscopic studies (e.g., see the comprehensive listing compiled by Gopka et al. 2004, their Table 1). As first noted by Wallerstein et al. (1963), the star is metal-deficient. Recent estimates of the metallicity are in the range $-2.20 < [\mathrm{Fe/H}] < -1.96$.[10] Included in the *n*-capture abundance study by Gilroy et al. (1988), HD 221170 has long been recognized as an *r*-process–rich star and has often been utilized as a template metal-poor star observation in other programs, including those of Burris et al. (2000), Fulbright (2000), Mishenina & Kovtyukh (2001), Mishenina et al. (2002), Yushchenko et al. (2002), Simmerer et al. (2004), and Barklem et al. (2005). In this paper we describe our observations and analysis and compare our results with previous observations, with scaled solar *r*-process predictions, and with other *r*-process–rich stars, concluding with discussions regarding the nucleocosmochronometric age of HD 221170 and *r*-process sites.

2. OBSERVATIONS AND REDUCTIONS

We gathered new high-resolution, high signal-to-noise ratio (S/N) spectra of HD 221170 with the High Resolution Echelle Spectrometer (HIRES; Vogt et al. 1994) on the Keck I telescope at the W. M. Keck Observatory and with the "2d-coudé" échelle spectrograph (Tull et al. 1995) on the 2.7 m H. J. Smith telescope at McDonald Observatory.

We observed HD 221170 with HIRES at Keck I using a blue configuration (HIRESb) and the new three-chip mosaic of MIT-LL CCDs. Using the same setup as that described in Ivans et al. (2005), we obtained essentially continuous wavelength coverage in the range $\sim$3050 Å $\leq \lambda \leq$ 5895 Å and a resolving power of $R \equiv \lambda/\Delta\lambda \simeq 40{,}000$. Spectra of the hot rapidly rotating star δ Cet aided in the division of telluric features in the reddest wavelengths and also served as a check on the data reduction of the bluest orders of the spectrum of HD 221170. Four exposures of HD 221170 were taken to attain a co-added S/N of 85:1 per resolution element at 3200 Å, increasing redward, to $\sim$120 at 3520 Å, $\sim$140 at 3900 Å, $\sim$260 at 5100 Å, and $\sim$290 at 5900 Å. Data reduction was performed using standard tasks in IRAF[11] including bias subtraction, bad pixel interpolation, wavelength calibration, and co-addition of the one-dimensional spectra; in FIGARO[12] including flat-fielding, light cosmic-ray excision, sky and scattered light subtraction, and extraction of the one-dimensional spectra; and in SPECTRE (Fitzpatrick & Sneden 1987) for final processing including continuum normalization and telluric feature division.

As part of the Simmerer et al. (2004) survey of La and Eu abundances over a large metallicity range, data for HD 221170 were also gathered with the McDonald Observatory 2d-coudé échelle spectrograph in the wavelength range 3800 Å $< \lambda <$ 7800 Å. The spectrum is continuous in the range $\lambda <$ 5800 Å, with some losses to order interstices at redder wavelengths. We also acquired a spectrum of the hot, rapidly rotating star ζ Aql for use in canceling the yellow and red telluric features of O_2 and H_2O. The spectrograph setup yielded $R \simeq 60{,}000$. Data reduction was performed using standard tasks in IRAF and SPECTRE. We refer the reader to Simmerer et al. (2004, their § 2) for further details regarding the spectrograph setup and data reduction of the 2d-coudé observations. The co-added reduced 2d-coudé spectra have S/N > 260 for $\lambda >$ 5900 Å, and this declines steadily to levels of 80 at $\lambda =$ 4000 Å.

In Figure 1 we display selected spectrum swaths for our data sets in overlapping spectral regions. Two of us independently reduced the Keck and McDonald spectra, employing different methods and completely different software for the removal of scattered light and cosmic-ray contributions. The resulting spectra are in excellent agreement. The selected features in this figure are the same as those displayed by Yushchenko et al. (2002, their Fig. 2) and Yushchenko et al. (2005, their Figs. 1–4). Their 2005 investigation is based on high-S/N, $R \simeq 45{,}000$ data gathered at the 2.0 m Zeiss telescope at the Peak Terskol Observatory with the coudé échelle spectrometer (Musaev et al. 1999) and should be comparable to our Keck spectrum. However, the appearance of our spectra does not compare favorably with those displayed

[10] We adopt the usual spectroscopic notation that for elements A and B, $\log \epsilon(\mathrm{A}) \equiv \log_{10}(N_\mathrm{A}/N_\mathrm{H}) + 12.0$ and $[\mathrm{A/B}] \equiv \log_{10}(N_\mathrm{A}/N_\mathrm{B})_\star - \log_{10}(N_\mathrm{A}/N_\mathrm{B})_\odot$. For example, $(N_\mathrm{Ho}/N_\mathrm{Fe})_\star = 5(N_\mathrm{Ho}/N_\mathrm{Fe})_\odot \Rightarrow [\mathrm{Ho/Fe}] = +0.7$. Also, metallicity in our discussions refers to the normalized iron abundance, the stellar [Fe/H] value.

[11] IRAF is distributed by the National Optical Astronomy Observatory, which is operated by the Association of Universities for Research in Astronomy, Inc., under cooperative agreement with the National Science Foundation.

[12] FIGARO is provided by the Starlink Project, which is run by CCLRC on behalf of PPARC (UK).

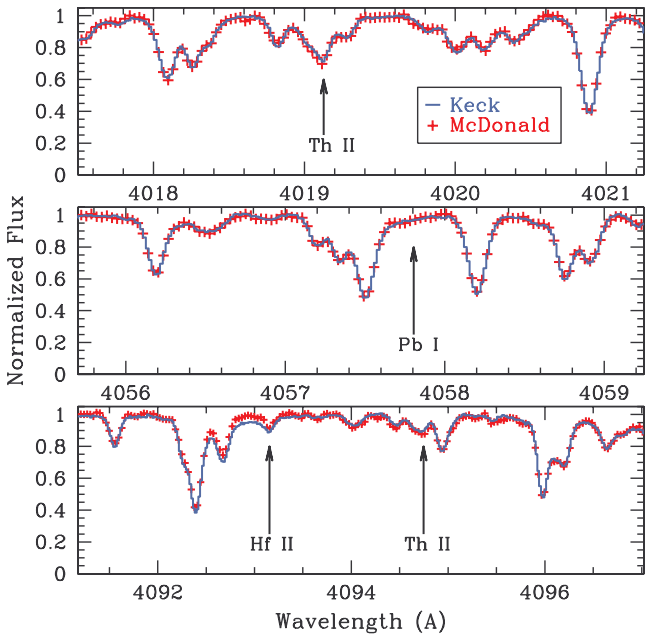

FIG. 1.—Examples of the reduced spectra taken with the Keck HIRESb (*blue solid line*) and McDonald 2d-coudé spectrographs (*red plus signs*) for a sample of the wavelength regions displayed by Yushchenko et al. (2002, their Fig. 2) and Yushchenko et al. (2005, their Figs. 1–4): Th II at 4019.13 Å, Pb I at 4057.81 Å, Hf II at 4093.16 Å, and Th II at 4094.75 Å.

in the Yushchenko et al. (2005) study. Neither do our Keck and McDonald data sets match well the spectrum displayed in the study by Gopka et al. (2004), who based their investigation on previously acquired Peak Terskol data, as well as high-S/N, $R \simeq 60{,}000$ data gathered with the ELODIE échelle spectrograph (Soubiran et al. 1998) on the 1.9 m telescope of the Observatoire de Haute Provence. In addition, Figure 1 of Gopka et al. (2004) shows that the Peak Terskol and ELODIE data appear to be in less than good agreement with each other. However, all data sets in this discussion are purportedly of high (100–250) S/N; the cause of the mismatches is unclear.

Carney et al. (2003, their Table 4) find that HD 221170 has possessed a constant radial velocity during the 14 yr spanned by their observing program. This star does not appear to have a companion. The four data sets under discussion here were gathered over a number of years, with those of this study taken more than 3 yr apart (ELODIE, prior to 1998; McDonald, 2001 July; Peak Terskol, 2002 June; and Keck, 2004 October). It is highly unlikely that the data belong to a variable star. We do not have an explanation for either (1) the difference between the appearance of the two (Gopka et al. 2004) data sets or (2) the difference between the Gopka et al. (2004)/Yushchenko et al. (2005) data sets and the spectra employed in this study. Further comments on these differences are given in § 5.

3. ANALYSIS

Our abundance analysis relied on the results of a combination of spectrum syntheses and equivalent width (EW) analyses. We relied on the Keck HIRESb data for wavelengths in the range $\sim$3050 Å $\leq \lambda \leq$ 5895 Å and on the McDonald 2d-coudé data for redder wavelengths. In overlapping wavelength regions, both data sets were checked in the analyses of particularly weak or noisy features. For each spectral order, the continuum was set by interactively fitting a spline function to line-free spectral regions. Locating the continuum was aided by comparing the spectra of our program stars with those of the Arcturus atlas (Griffin 1968), as well as spectrum syntheses. The following subsections describe the line lists we used, the measurements we performed, the solar abundances we adopted, the methods we employed, and the stellar parameters and abundances we derived in this study.

TABLE 1

ABUNDANCES DERIVED FROM INDIVIDUAL FEATURES

Ion (1)	λ (Å) (2)	χ (eV) (3)	log gf-Value (4)	EW[a] (mÅ) (5)	log ϵ(X) (6)	[X/Fe][b] (7)	Notes (8)
$\log \epsilon(\mathrm{C})_\odot = 8.56$ ($Z = 6$)[c]							
I	CH band	...	...	Syn	5.67	−0.71	...
$\log \epsilon(\mathrm{N})_\odot = 8.05$ ($Z = 7$)							
I	CN band	...	...	Syn	6.46	+0.59	...
$\log \epsilon(\mathrm{O})_\odot = 8.93$ ($Z = 8$)							
I	6300.31	0.00	−9.750	Syn	+6.97	+0.22	...
	6363.79	0.02	−10.250	Syn	+6.97	+0.22	...
$\log \epsilon(\mathrm{Na})_\odot = 6.33$ ($Z = 11$)							
I	5682.63	2.10	−0.699	Syn	+3.89	−0.26	...
	5688.00	2.10	−0.456	Syn	+3.95	−0.20	HFS
	5889.95	0.00	+0.112	220.2	...	...	[d]
	5895.92	0.00	−0.191	212.3	...	...	[d]

NOTES.—These results are based on Keck HIRESb spectrum features for wavelengths in the range $\sim$3050 Å $\leq \lambda \leq$ 5895 Å and McDonald 2d-coudé spectrum features for redder wavelengths. See § 3. Table 1 is published in its entirety in the electronic edition of the *Astrophysical Journal*. A portion is shown here for guidance regarding its form and content.

[a] In the place of an EW measurement, "Syn" denotes a feature for which our derived abundance relies on a spectrum synthesis computation.

[b] The abundances derived for an individual feature relative to the scaled solar value: [Fe I/H], [Fe II/H], or [X/⟨Fe⟩] with ⟨[Fe/H]⟩ = −2.18. Upper limits are denoted "limit."

[c] Derived $^{12}\mathrm{C}/^{13}\mathrm{C} = 7 \pm 2$.

[d] Excluded from analysis (nonnegligible non-LTE correction required).

3.1. *Equivalent Width Measurements*

In Table 1 we list relevant data for all of the transitions employed in this study. The elements are listed in order of atomic number (Z), and for each element, the values for neutral species precede those of the ionized ones and are otherwise listed in order of increasing wavelength.

Parameters for the individual transitions (λ, χ, log gf, and EW) are presented in columns (2)–(5). The EWs were measured with SPECTRE, either using direct integration of the flux across an observed line profile or adopting a Gaussian approximation (for all but the strongest lines, for which Voigt profile fits were employed). Most of the EW measurements are of neutral iron lines with atomic parameters adopted from O'Brian et al. (1991). Supplementing these lines are features we have employed in other high-resolution abundance studies of globular cluster red giant stars (e.g., Ivans et al. 2001; Sneden et al. 2004; Johnson et al. 2006), *r*-process–enriched metal-poor stars such as BD +17 3248 and CS 22892−052 (e.g., Cowan et al. 2002; Sneden et al. 2003), and other field stars with metallicities comparable to that of HD 221170 (e.g., Ivans et al. 2003), supplemented by recent laboratory results (e.g., Nilsson et al. 2006). Additional notes regarding specific elements are discussed further in § 3.3.

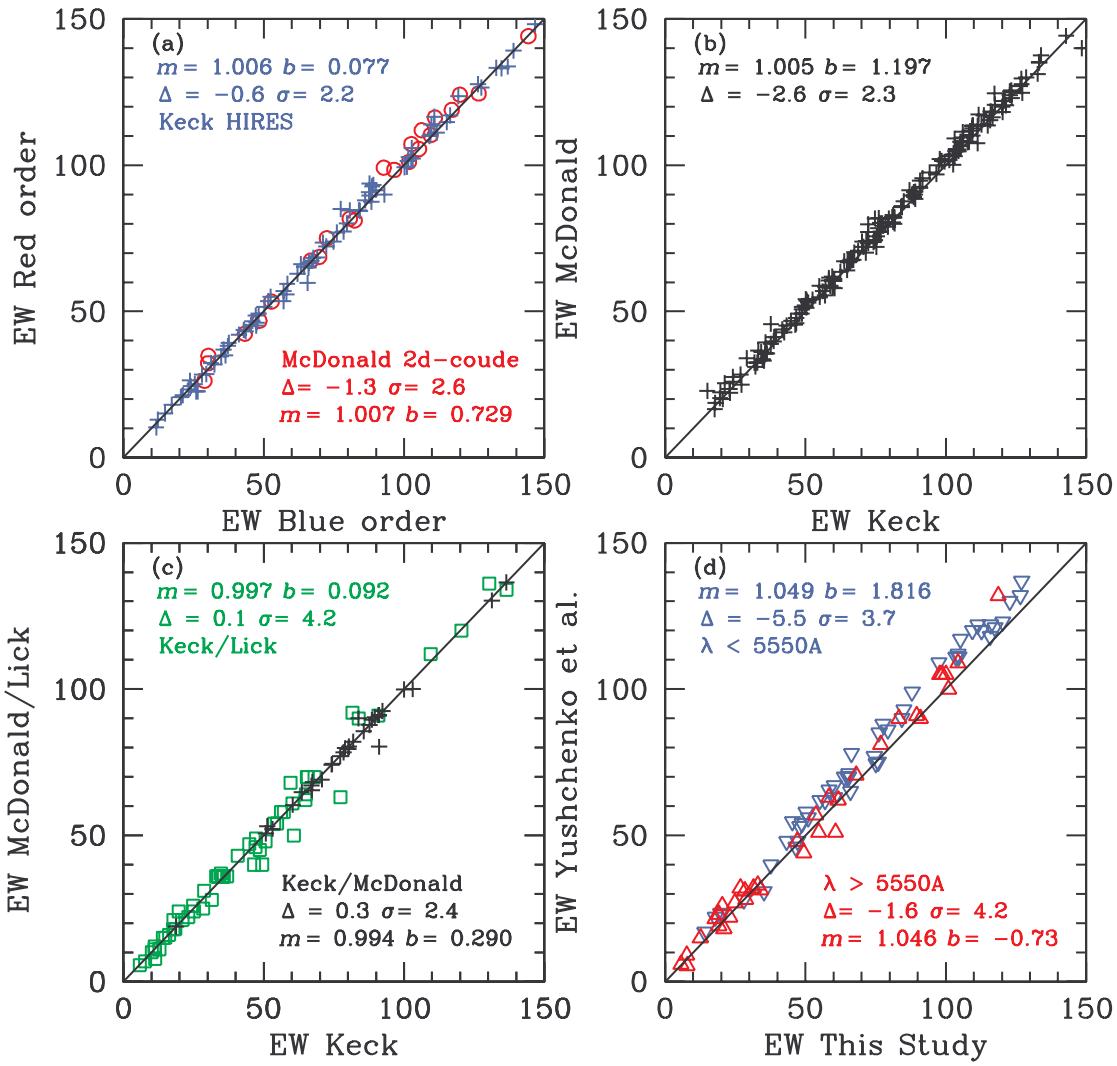

FIG. 2.—Comparisons of EWs for lines in common between the data sets discussed in § 2. (*a*) Overlapping orders within the Keck and McDonald data sets (*blue plus signs and red circles, respectively*); (*b*) lines in common in the Keck and McDonald data sets; (*c*) independently measured McDonald EWs (*black plus signs*) and Lick EWs (Fulbright 2000; *green squares*) vs. Keck EWs; (*d*) lines in common with Yushchenko et al. (2005), color-coded by $\lambda < 5550$ (*blue downward-pointing triangles*) or >5550 Å (*red upward-pointing triangles*). In all panels, we show the values of the slope (*m*) and zero-point shifts (*b*) of the regressions (where the solid line represents a one-to-one relation), along with the mean differences (Δ) and standard deviations of the measurements (σ). The values were derived employing all EWs in common; the panel displays are restricted to EWs <150 mÅ.

In Figure 2 we compare the EWs measured in the Keck HIRESb and McDonald 2d-coudé data sets. As illustrated (as well as quantitatively described in this figure), the data reduction and EW measurements in this study appear to have been performed consistently. For instance, in Figure 2*a*, considering the Keck and McDonald spectra independently, we show comparisons between EWs of the same lines appearing on adjacent échelle orders that overlap in wavelength (i.e., the EW from the bluer order is compared against the EW obtained in the redder order). In Figure 2*b*, EWs of lines in common between the Keck and McDonald spectra measured by the same person are compared. In Figure 2*c*, our Keck HIRES EWs are compared with independently measured McDonald 2d-coudé (Simmerer et al. 2004) and Lick Hamilton (Fulbright 2000) EWs. These three panels demonstrate the accuracy of our EWs both internally and externally, despite the numerous differences in spectrographs, data reduction and measurement tools, and techniques employed by three independent observers. However, the same cannot be said of the data of Figure 2*d*, showing an EW comparison between this study and that of Yushchenko et al. (2005, their Table 1). The EW differences are large and also appear to be wavelength dependent: they are largest in the blue wavelength regions where most of the *n*-capture features are to be found. We are unable to explain the EW differences between Yushchenko et al. (2005) and either (1) our study or (2) an independent set of EWs measured from data acquired with the Lick Hamilton échelle spectrograph (Fulbright 2000). Further comments on these differences are given in § 5.

3.2. *Stellar Atmosphere Model and Parameters*

We employed stellar atmospheres without overshooting (Castelli & Kurucz 2003), using a modified interpolation code supplied by A. McWilliam (2001, private communication). We performed the abundance calculations with a current version of the LTE stellar line analysis code, MOOG (Sneden 1973). Initial stellar parameters were determined employing photometry from SIMBAD and the Two Micron All Sky Survey (2MASS); the extensions of the color-$T_{\rm eff}$ calibrations of Alonso et al. (1996, 1999) by Ramírez & Meléndez (2005), using a software program supplied by I. Ramírez (2005, private communication); the value of

$E(B-V) = 0.14$ from the dust map calibrations of Schlegel et al. (1998); and a parallax of 2.30 ± 0.84, as measured by *Hipparcos* (Perryman et al. 1997).

Utilizing the EW measurements presented in Table 1, we then iterated on the Fe abundances to eliminate abundance trends with respect to the excitation potentials (setting $T_{\rm eff}$; see, e.g., Kraft & Ivans 2003), EWs (setting the microturbulent velocity, ξ_t), and ionization state (setting $\log g$). The initial $T_{\rm eff}$ value of 4610 K presented abundance trends with the values of the excitation potentials of the lines, indicating that the photometric $T_{\rm eff}$ was too warm. This is likely a result of too high a value for $E(B-V)$; in contrast, the Burstein & Heiles (1982) value is less than half that of Schlegel et al. (1998).

Employing spectroscopic constraints, we derived final parameter values of ($T_{\rm eff}$, $\log g$, ξ_t, [Fe/H]) = (4510, 1.00, 1.8, −2.19). Since the predicted range of $E(B-V)$ is so large (0.06–0.14 dex, with a mean of 0.1), we are satisfied with the $E(B-V) = 0.095$ implied by the stellar parameters we derived by the spectroscopic constraints, which are independent of the photometry. This reddening value, combined with an assumed stellar mass of $0.8\ M_{\odot}$ and the $\log g$-value we derived, yields a spectroscopically derived distance of 675 pc, on the far side but within the parallax errors of the *Hipparcos* measurement. Our derived parameters are also within the range of stellar parameters employed in previous CCD-based studies as listed in Gopka et al. (2004; their Table 1: 4410 K $< T_{\rm eff} <$ 4686 K, $0.75 < \log g < 1.57$, 1.5 km s^{-1} $< \xi_t <$ 2.7 km s^{-1}, and $-2.19 <$ [Fe/H] < -1.79). Using spectroscopic constraints similar to those we employed, the Gopka et al. (2004) study derived values of ($T_{\rm eff}$, $\log g$, ξ_t, [Fe/H]) = (4475, 1.0, 1.7, −2.03). Yushchenko et al. (2005) remeasured the iron abundance and used the parameters (4475, 1.0, 1.7, −2.09) in their analysis, parameters in good agreement with the values we have derived.

Our adopted solar abundances for each element are listed in Table 1, preceding the transition information. With the exception of iron and some *n*-capture elements, our analysis relies on the solar photospheric (where reliable) or meteoritic abundances from the critical compilation of Anders & Grevesse (1989). As in previous studies by our group, we adopt $\log \epsilon({\rm Fe}) = 7.52$, a value close to that recommended by Grevesse & Sauval (1998) [$\log \epsilon({\rm Fe}) = 7.50$]. We refer the reader to discussions by Sneden et al. (1991), Ryan et al. (1996), and McWilliam (1997), where some of the alternative solar iron abundance choices are summarized. In the element range of $57 < Z < 67$, the solar abundances for six of the elements have been recently redetermined, employing new and improved laboratory measurements of atomic parameters, and we adopt those solar abundances in this study (La, Lawler et al. 2001a; Nd, Den Hartog et al. 2003; Sm, Lawler et al. 2006; Eu, Lawler et al. 2001c; Tb, Lawler et al. 2001b; Ho, Lawler et al. 2004).

3.3. *Abundance Analysis Methodology*

HD 221170 is a cool star with a strong-lined spectrum. As such, it has revealed many more *n*-capture transitions than we have previously worked with in studies of *r*-process–enriched metal-poor stars, such as CS 22892−052 (Sneden et al. 2003), BD +17 3248 (Cowan et al. 2002), and HD 115444 (Westin et al. 2000). For many elements in this study, we have significantly expanded the number of transitions employed in our analysis. However, we have endeavored to employ single-source and recent *gf*-values wherever possible in order to diminish the uncertainties involved by combining studies that may not be on the same *gf*-value system. Happily, many of the *n*-capture element species detectable in metal-poor stars have been subjected to extensive laboratory investigations within the past two decades. For most elements considered here, we have only employed *gf*-values determined in these recent laboratory efforts. The exceptions are noted below in § 3.4. Laboratory transition probabilities were adopted without change for the *n*-capture lines of interest in each line list.

TABLE 2
Sc II and Mn I Line Lists

λ (Å)	Species	χ (eV)	$\log gf$-Value[a]
4400.379	Sc II	0.605	−2.019
4400.383	Sc II	0.605	−1.821
4400.383	Sc II	0.605	−1.196
4400.387	Sc II	0.605	−1.767
4400.387	Sc II	0.605	−1.429
4400.390	Sc II	0.605	−1.793
4400.390	Sc II	0.605	−1.720
4400.392	Sc II	0.605	−2.019
4400.393	Sc II	0.605	−1.894
4400.393	Sc II	0.605	−2.113

Notes.—Table 2 is published in its entirety in the electronic edition of the *Astrophysical Journal*. A portion is shown here for guidance regarding its form and content.

[a] Hyperfine structure information adopted from Kurucz & Bell (1995), with $\log gf$-values normalized to those adopted in this study (see § 3.1).

Abundances were derived from EW measurements for those transitions that we judged to be unblended and able to be modeled as single spectral features. The exception to this rule was in our treatment of the clean and easily measured Sc and Mn lines of HD 221170, in which the features are broadened by hyperfine structure (HFS) splitting. HFS results from nucleon-electron spin interactions in odd-*Z* atoms, splitting absorption lines into multiple components. The multicomponent structure permits the line to grow to a greater strength before saturating. Without accounting properly for HFS, abundances quoted by other studies for elements sensitive to HFS can be severely overestimated. For example, in HD 221170, including HFS makes a difference of 0.35 dex in the derived $\log \epsilon({\rm Mn})$ abundance for the Mn I feature at 4030.76 Å. For further discussion on the importance of including HFS, see, e.g., Gratton (1989), McWilliam et al. (1995), Ryan et al. (1996), and Prochaska & McWilliam (2000). In our analysis of Sc and Mn, we relied on the extensive HFS splitting lists produced by Kurucz & Bell (1995),[13] and our resulting line list is given in Table 2.

Many of the *n*-capture features of interest also have HFS and/or multiple naturally occurring isotopes with measured wavelength differences ($\Delta\lambda \gtrsim 0.01$ Å). Notes regarding whether HFS/isotopic splitting was accounted for in a given feature are presented in column (8) of Table 1. In addition, nearly all of the strongest *n*-capture transitions occur in the complex blue–UV spectral region ($\lambda \lesssim 4500$ Å), where blended features are the rule, not the exception. Therefore, for more than half of the *n*-capture lines we employed full synthetic spectra in the analyses. In most cases a spectral region of 4–8 Å surrounding each synthesized line was considered. As in our prior studies, we initially formed the line lists for the synthetic spectra from the neutral and first ionized atomic transitions with lower excitation potentials $\chi < 7$ eV found in the Kurucz (1998) atomic and molecular line database.[14] In spectral regions with significant molecular hydride and cyanogen

[13] The HFS lists are available at http://kurucz.harvard.edu/linelists/gfhyperall.

[14] Available at http://kurucz.harvard.edu.

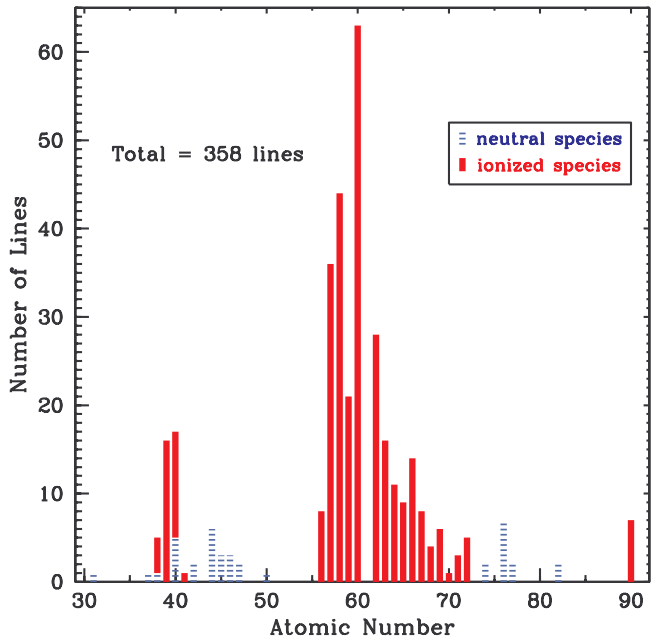

FIG. 3.—Number of transitions used in determining the abundances of the *n*-capture elements. Blue dashed histograms and red solid histograms represent, respectively, neutral and first ionized species, as given in the figure legend.

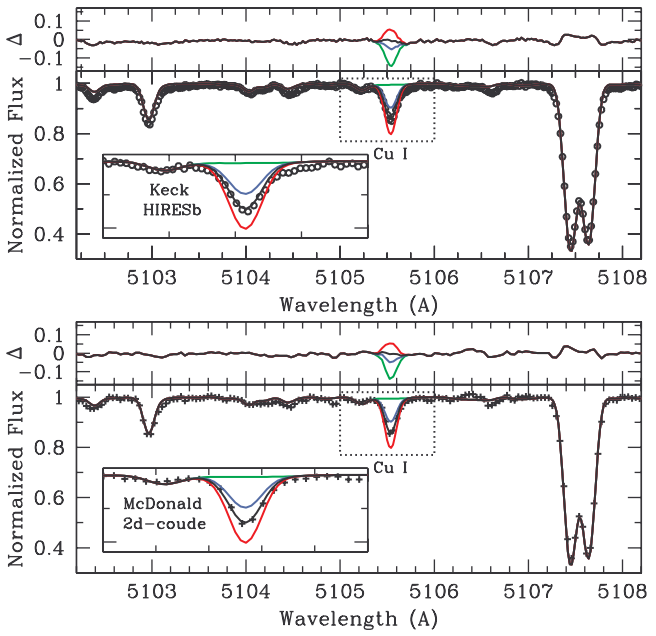

FIG. 4.—Observed and synthetic spectra of Cu I in HD 221170. The 6 Å swaths shown here illustrate the typical match between both the Keck HIRESb (*circles*) and McDonald 2d-coudé (*plus signs*) spectra and the syntheses obtained from the stellar and smoothing parameters described in §§ 3.2 and 3.3. The Δ panels above each of the syntheses illustrate the differences to the respective fits. The inset illustrates a region 1 Å wide surrounding the feature at 5105.5 Å, as denoted by the dotted lines in the main panels. The solid lines represent synthetic spectra with variation only in the assumed Cu abundance. The black line shows the best fit between the synthetic and observed spectra. The red and blue lines show the change in the Cu I feature with changes of ±0.2 dex in assumed Cu abundance, respectively, and the green lines show the synthetic spectrum without any Cu contribution.

absorption features, parameters for these lines also were taken from the Kurucz database, but for hydrides the lower excitation potential cutoff was $\chi \sim 1.5$ eV. These lines were occasionally supplemented by other transitions identified in the solar spectrum by Moore et al. (1966). In accord with our previous work on spectrum syntheses of *n*-capture elements, the transition probabilities of a few contaminant lines in some spectral intervals were adjusted to provide best matches to solar/stellar spectra, employing the Kurucz et al. (1984) solar flux atlas, and the solar model atmosphere of Holweger & Müller (1974). On rare occasions we added an arbitrarily assumed Fe I line to account for weak contaminants in the wings of the spectral features of interest.

We convolved the raw synthetic spectra generated from these line lists with Gaussian functions whose FWHM values matched the observed spectra. We empirically determined an $\mathrm{FWHM}_{\mathrm{total}}$ of 0.10–0.11 Å at $\lambda \approx 4000$ Å, which is in accord with the expected value from the convolution of the known spectrograph resolution and macroturbulent velocity. Then synthetic and observed spectra with varying abundances of the elements under scrutiny were iteratively compared until the best average abundance was found for each feature.

More than 350 transitions of 35 species have yielded abundances for 30 *n*-capture elements and significant upper limits for three others. Well-determined abundances involving large numbers of transitions based on the best laboratory atomic data require little comment. In Figure 3 we plot a histogram of the number of lines employed for each *n*-capture species. Unsurprisingly, the peak of this distribution occurs for the rare earth elements, whose first ions present many detectable transitions in the visible and near-UV spectral regions.

3.4. *Comments on Abundance Derivations of Individual Elements*

In this subsection we concentrate on those species that deserve special attention, either to support our abundance claims or to provide some cautionary statements. Only brief notes are given for most elements. However, since the claimed significant departures of HD 221170 *n*-capture abundances from scaled solar system values rest mainly on the elements Hf, Pb, and Th, they receive more extended discussion.

CNO *group* (*carbon:* $Z = 6$, CH; *nitrogen:* $Z = 7$, CN; *oxygen:* $Z = 8$, [O I]).—Abundances of the CNO group provide clues to the nucleosynthetic history of HD 221170. In addition, the molecular species formed from these elements are important contributors to the overall line absorption surrounding and blending with other features of interest in this study, such as Th. The C and N abundances here were derived from the CH $A\,^2\Delta$–$X\,^2\Pi$ G band and the CN $B\,^2\Sigma^+$–$X\,^2\Sigma^+$ (0, 0) vibrational band. We derive a carbon isotope ratio of $^{12}\mathrm{C}/^{13}\mathrm{C} = 7 \pm 2$, in agreement with Yushchenko et al. (2005), who noted their agreement with Sneden et al. (1986). Our oxygen abundances were derived from full synthetic spectrum computations of the [O I] λλ6300, 6363 lines. The construction of the line lists employed is as described by Sneden et al. (1991) and Westin et al. (2000).

Copper ($Z = 29$, Cu I).—The copper abundance for HD 221170 was investigated employing the techniques and line lists employed in the extensive globular cluster giant star study of Simmerer et al. (2003). Unfortunately, the Cu feature at 5782 Å could not be utilized here. The large radial velocity of HD 221170 shifts the λ5782 feature into the well-known λ5780 diffuse interstellar band (see, e.g., Herbig 1975). The small-scale structure of this broad band compromised our synthetic spectrum fit to the profile of the Cu I line, so we dropped it from further consideration. Our Cu abundance therefore is derived exclusively from the spectrum synthesis match to the λ5105 feature, as displayed in Figure 4.

Rubidium ($Z = 37$, Rb I).—Only the resonance line of Rb I at 7800.29 Å is strong enough to attempt analysis in metal-poor

stars. We adopted the *gf*-value recommended by Fuhr & Wiese (2005). Our claimed detection of this very weak feature should be viewed with caution, as we do through the assignment of a large abundance uncertainty value.

Strontium ($Z = 38$, Sr I, Sr II).—The resonance line of Sr I at 4607.3 Å is detected and apparently suffers from little blending in the HD 221170 spectrum. Adopting the *gf*-value of Migdalek & Baylis (1987), synthesis of this line yields an abundance about 0.4 dex lower than that determined from four lines of Sr II. This problem has been noted previously in stellar and solar spectra. The reader is referred to Gratton & Sneden (1994) for further discussion. Our adopted Sr II *gf*-values are those recommended by Fuhr & Wiese (2005).

Yttrium ($Z = 39$, Y II).—The initial analysis based on EW measurements yielded an unacceptably large line-to-line abundance scatter. Therefore, our final values were derived from synthetic spectra, with full accounting of HFS in the Y II lines. The hyperfine constants were taken from Dinneen et al. (1991), Nilsson et al. (1991), Villemoes et al. (1992), Wännström et al. (1994), and Persson (1997). The resulting three to four components to each line have only small wavelength differences (always $\lesssim$0.003 Å), so changes to the derived Y abundances were less than or comparable to basic measurement uncertainties in our spectra. However, better estimation of blending features to the Y II features brought reasonable internal abundance agreement, $\sigma = 0.07$, among the 16 lines of this study. All *gf*-values employed here are adopted from the Hannaford et al. (1982) study.

Zirconium ($Z = 40$, Zr I, Zr II).—Yushchenko et al. (2005) detected Zr I transitions in HD 221170, the first time this species has been identified in very metal-poor stars. Employing the *gf*-values from Biémont et al. (1981), we confirm the existence of the two lines Yushchenko et al. (2005) found, add three more lines detectable on our spectra, and derive a mean Zr abundance (albeit with relatively large line-to-line scatter) that is in excellent agreement with the value determined from Zr II.

Niobium ($Z = 41$, Nb II).—This abundance has been derived from a single detectable line, which unfortunately lies in a crowded near-UV spectral region where also the stellar flux is relatively low. We adopted the *gf*-value from Hannaford et al. (1985). The line has broad HFS, which we accounted for empirically by splitting it into a number of substructure components to approximately match an emission-line profile from the National Solar Observatory Fourier transform spectrometer (FTS) archives. A larger error bar was assigned to this abundance.

Molybdenum ($Z = 42$, Mo I).—We adopted the *gf*-values of Whaling & Brault (1988). In § 3.2.1 of Sneden et al. (2003), there is an extended discussion of the detection and analysis of the λ3864.10 line in CS 22892−052. The observed feature can be attributed to a combination of Mo I, CH, CN, and other atomic transitions, but Sneden et al. (2003) argued that a reliable Mo abundance could be obtained for that star. The molecular contaminants for the λ3864 line are weaker in HD 221170 than they are in CS 22892−052 because its C abundance is smaller, and the atomic contaminants also appear to be not strong in HD 221170. Confirmation of the presence of Mo comes from the detection of Mo I λ3798.25. This line lies too close to the H I Balmer line at 3797.90 Å to yield a trustworthy abundance by itself, but our best estimate is very consistent with the abundance derived from the λ3864 line, bolstering our confidence in the mean Mo abundance. Both of our Mo I features are displayed in Figures 5*a* and 5*b*.

Ruthenium ($Z = 44$, Ru I).—The *gf*-values for all six lines were adopted from Wickliffe et al. (1994). Two representative features are displayed in Figure 5*b*.

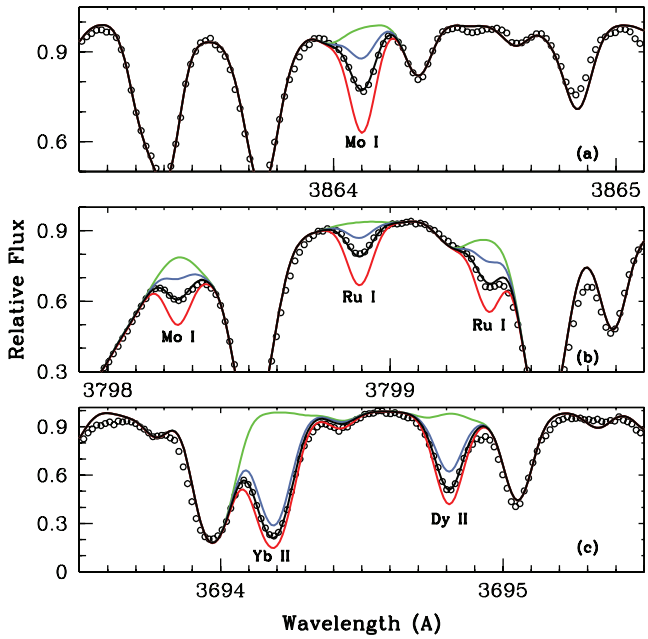

FIG. 5.—Selected spectra of *n*-capture elements in the near-UV wavelength region. Open circles represent the observed Keck HIRESb spectra. The solid lines represent synthetic spectra with variation only in the assumed abundance of the noted species. The black line shows the best fit between the synthetic and observed spectra with the abundance for each species given in col. (6) of Table 1. The red and blue lines show the change in the features with changes of ±0.4 dex in assumed abundance, respectively, and the green line shows the synthetic spectrum without any contribution from the species noted. In (*b*), the Mo I line is clearly detected but lies in the middle of a complex blend of Fe I and H I features. The abundance from this line is consistent with the cleaner Mo I λ3864.1 line but should be interpreted with caution.

Rhodium ($Z = 45$, Rh I).—The lines at 3692.4 and 3700.9 Å, with transition probabilities from Duquette & Lawler (1985), yield abundances that are in poor agreement: $\log \epsilon = -0.55$ and -0.10, respectively. A relatively clean line in the HD 221170 spectrum at 3434.9 Å not done by Duquette & Lawler (1985) was included in the Kwiatkowski et al. (1982) laboratory investigation. The transition probability scales of these two studies are in good agreement: for nine lines in common, $\langle \Delta \log gf \rangle = +0.03 \pm 0.04$ ($\sigma = 0.11$) in the sense Duquette & Lawler (1985) minus Kwiatkowski et al. (1982). Adopting the latter's $\log gf$ yields $\log \epsilon = -0.40$ for the λ3434.9 line.

Palladium ($Z = 46$, Pd I).—The *gf*-values were adopted from Biémont et al. (1982).

Silver ($Z = 47$, Ag II).—The resonance lines have reliable transition probabilities. We adopted the values recommended by Fuhr & Wiese (2005), which are in good agreement with the values determined by Cunningham & Link (1967). See Ross & Aller (1972) for further references and hyperfine/isotopic substructure discussion.

Tin ($Z = 50$, Sn I).—We were able to derive an upper limit for the feature at 3801.02 Å employing the *gf*-value recommended by Fuhr & Wiese (2005).

Barium ($Z = 56$, Ba II).—In previous work by our group on selected Ba features we have performed blended-line EW analyses that included both hyperfine and isotopic subcomponents adopted from McWilliam (1998), with values of $\log gf$-value normalized to those adopted in our previous work (e.g., Ivans et al. 1999). As discussed in § 3.3, however, in HD 221170 the *n*-capture material is sufficiently enhanced that blending from other *n*-capture lines becomes significant in many features (e.g.,

in the Ba II λ4130 feature from Ce II). A blended-line EW analysis of Ba in HD 221170 was therefore deemed untrustworthy and a full spectrum synthesis was performed on each feature. The transition probabilities employed here are slightly different than those adopted in our previous papers. A critical compilation of transition probabilities for both Ba I and Ba II has been published by Klose et al. (2002), and we adopt their recommended values.

We attempted to detect Ba I λ5535.5, the only strong line of this species. Unfortunately, this line is dominated in the solar spectrum by a pair of Fe I transitions, and the Ba contribution to the blend could not be distinguished in our HD 221170 spectrum.

Lanthanum ($Z = 57$, La II).—Some features of La II have notable HFS and required updated calculations to be made of the HFS patterns. In the Appendix we provide the results of these calculations for 30 of the 36 La II features employed in this study. Although upper level hyperfine constants are not available for the remaining six, the profiles of these six lines were inspected on high-resolution laboratory FTS data from Lawler et al. (2001a). The broadening induced by HFS for these lines is not as large as the broadenings of the other 30 La II lines and is not sufficiently resolved in the FTS data to derive a precise measure of the HFS constants. The effect of the (weak) HFS splitting for these lines was, however, included (approximately) in the analysis of the stellar spectra. The complete HFS patterns from the best available HFS constants are included for the other 30 La II lines in the Appendix.

Cerium ($Z = 58$, Ce II).—Abundances derived for all 44 lines relied on the *gf*-values of Palmeri et al. (2000).

Praseodymium ($Z = 59$, Pr II).—All 21 features were analyzed employing the *gf*-values of Ivarsson et al. (2001).

Neodymium ($Z = 60$, Nd II).—We performed 63 abundance measurements employing the extensive line list of Den Hartog et al. (2003).

Samarium ($Z = 62$, Sm II).—Accurate experimental log *gf*-values have been newly determined for over 900 Sm II lines by Lawler et al. (2006). The reader is referred to that paper for new determinations of the Sm abundances in the Sun and the *r*-process–rich stars CS 22892−052, HD 115444, and BD +17 3248.

Europium ($Z = 63$, Eu II).—We employed the *gf*-values derived by Lawler et al. (2001c). Updated energy levels for Eu II and complete HFS and isotopic patterns are included in the Appendix for 24 Eu II lines. The important low-lying even- and odd-parity Eu II levels were measured to FTS (interferometric) accuracy of ± 0.003 cm^{-1}.

For this *r*-process–dominated element, there are two naturally occurring isotopes whose abundance fractions are fr(^{151}Eu) $\equiv$ ^{151}Eu/(^{151}Eu + ^{153} Eu) = 0.478 and fr(^{153}Eu) = 0.522 in solar system material (see, e.g., the review of Lodders 2003 and references therein). Sneden et al. (2002) and Aoki et al. (2003) have demonstrated that the *r*-process–rich stars HD 115444, BD +17 3248, CS 22892−052, and CS 31082−001 also have approximately equal fractions of the two Eu isotopes. For HD 221170, we computed synthetic spectra of the $\lambda\lambda$3819.7, 4129.7, and 4205.0 lines with varying ^{151}Eu and ^{153}Eu fractional abundances and similarly find fr(^{151}Eu) $\approx$ fr(^{153}Eu) $\approx$ 0.5. However, since these most useful Eu isotopic abundance indicators are very strong in HD 221170 and are surrounded by complex atomic and molecular contaminants, this isotopic estimate is not tightly constrained, and the uncertainty in each abundance fraction is roughly ± 0.1.

Gadolinium ($Z = 64$, Gd II).—For these lines, we employed the *gf*-values of Bergström et al. (1988), supplementing these with some from the Kurucz (1998) database consistently normalized with the Bergström et al. (1988) values.

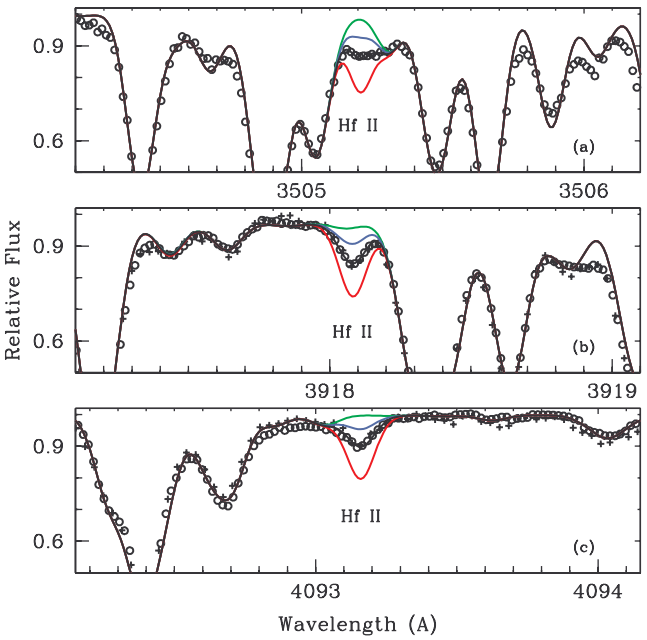

FIG. 6.—Observed and synthetic spectra of three Hf II lines in HD 221170. Open circles and plus signs represent the observed Keck HIRESb and McDonald 2d-coudé spectra, respectively. All lines are as in Fig. 5.

Terbium ($Z = 65$, Tb II).—The *gf*-values derived by Lawler et al. (2001b) were employed for all features.

Dysprosium ($Z = 65$, Dy II).—We adopted the *gf*-values from Wickliffe et al. (2000). A representative feature is displayed in Figure 5*c*.

Holmium ($Z = 67$, Ho II).—The abundances were derived employing the *gf*-values from Lawler et al. (2004).

Erbium ($Z = 68$, Er II).—We adopted the *gf*-values of Xu et al. (2003), preferring to limit our transition list to only the relatively few reported in that study rather than the larger numbers of Er II lines included in older laboratory studies. Of the many Er II lines, these are the only ones with sufficiently up-to-date parameters to be included in the Database of Rare Earths at Mons University (D.R.E.A.M.).[15] In addition, Er has four major naturally occurring isotopes whose HFS splitting has not been taken into account in any stellar abundance analyses to date. Thus, Er abundances are likely to have been overstated, with the reported associated uncertainties understated.

Thulium ($Z = 69$, Tm II).—Our abundance was derived employing the line list of Wickliffe & Lawler (1997).

Ytterbium ($Z = 70$, Yb II).—The *gf*-value was adopted from Biémont et al. (2002). The feature is displayed in Figure 5.

Lutetium ($Z = 71$, Lu II).—The upper limit was derived from three lines where *gf*-values from Fedchak et al. (2000) were employed.

Hafnium ($Z = 72$, Hf II).—Yushchenko et al. (2005) analyzed the $\lambda\lambda$3918.09 and 4093.16 lines and derived abundances that differed by 0.8 dex in log ϵ or 0.5 dex in [Hf/H]. In their § 3 they discussed this disagreement, arguing for its reality from significant EW differences: they measured $EW_{3918} = 45$ mÅ and $EW_{4093} = 15$ mÅ. They chose to use the mean abundance derived from these two lines for their final Hf value.

We have compared synthetic and observed spectra for these two lines and three other Hf II lines detected in our spectra, and in Figure 6 we display the data for the three most trustworthy

[15] The database is available at http://w3.umh.ac.be/~astro/dream.shtml.

features. For the $\lambda\lambda$3918 and 4093 lines (Figs. 6*b* and 6*c*, respectively), we have Keck and McDonald observed spectra of comparable quality, so both are plotted. The S/N of the McDonald spectrum is too low at 3505 Å to be useful in the analysis. Figure 6*c* can be compared to Figure 1 of Yushchenko et al. (2005). The Hf II lines in Figure 6 are all about the same strength, as they should be, given their excitation potentials and oscillator strengths listed in columns (2) and (3) of Table 1. The *gf*-values were adopted from Andersen et al. (1976). The EWs of the $\lambda\lambda$3918 and 4093 lines both are $\sim$15 mÅ. Our derived abundance for the λ4093 transition is in excellent agreement with the Yushchenko et al. (2005) value. Some problem probably exists in their spectrum of the λ3918 feature, and the small line-to-line scatter among the five lines employed in the present study lends some confidence in our derived mean Hf abundance, which is $\sim$0.3–0.4 dex smaller than that derived by Yushchenko et al. (2005).

Tungsten ($Z = 74$, W I).—Yushchenko et al. (2005) employed lines at 4008.7 and 4074.4 Å in their analysis. We also computed synthetic spectra of these lines, which should be the strongest of this element in the HD 221170 spectrum. We conclude that measurable W I absorption is probably present but both lines are so contaminated with other spectral features that it is difficult to derive a meaningful abundance. Here we describe the estimation of an upper limit.

The W I λ4008.75 line is heavily blended at least by Pr II λ4008.69, Ce II $\lambda\lambda$4008.67, 4008.73, and Nd II λ4008.75 (this line is of relatively high excitation potential and thus unlikely to contribute substantially). Inspection of the feature profile suggests that perhaps three transitions make up the total absorption. As might be expected, the overall spectral feature strength increases and decreases in rough proportion to the overall *n*-capture element content. Our syntheses suggest that the contaminants account for about $\frac{3}{4}$ of the total feature. The W I line is probably contributing to the absorption, and we formally derive $\log \epsilon(\mathrm{W}) \sim -0.6$, but the uncertainty in the W abundance derived from spectra with the resolution and S/N of our spectra must be very large (roughly $\pm$0.4 dex). The two Ce II lines have recently determined transition probabilities (Palmeri et al. 2000). The Pr II line was not included in the Ivarsson et al. (2001) laboratory study, and so we experimented with syntheses that did not include it. The observed feature is clearly not matched in this case, with an obvious gap at the Pr II line wavelength.

The λ4074.36 line is approximately a factor of 2 weaker than the λ4008 line. It too suffers blending, from the CH $B\,^2\Sigma^- - X\,^2\Pi$ (1–1) P_1 $J = 4.5$ λ4074.34 line (e.g., Bernath et al. 1991). Repeated trial syntheses, assuming the C abundance derived from the CH $A\,^2\Delta - X\,^2\Pi$ G band, suggest that the CH feature dominates here, and so $\log \epsilon(\mathrm{W}) \lesssim -1.0$. Complete neglect of the CH contaminant would lead to $\log \epsilon(\mathrm{W}) \approx -0.6$. We conclude that W I lines may have been detected in the spectrum of HD 221170 but probably cannot at this time be employed as reliable W abundance indicators. A conservative upper limit is $\log \epsilon(\mathrm{W}) \lesssim -0.6$, based on the *gf*-values of Den Hartog et al. (1987).

Osmium ($Z = 76$, Os I).—Ivarsson et al. (2003) transition probabilities were employed except for the λ4420.5 line, for which the log *gf*-value was determined by Kwiatkowski et al. (1984). We included this line because Ivarsson et al. (2003) also used it in their determination of the Os abundance of CS 31082−001.

Iridium ($Z = 77$, Ir I).—Our analysis relied on the *gf*-values of Ivarsson et al. (2003).

Lead ($Z = 82$, Pb I).—Yushchenko et al. (2005) derived their lead abundance from the λ4057.8 line. We have also used this transition along with that at 3683.5 Å, with both *gf*-values adopted from Biémont et al. (2000). The resulting abundances are in fair agreement, considering the weakness of the two lines and the blending problems of each (see Fig. 2 of Yushchenko et al. 2005).

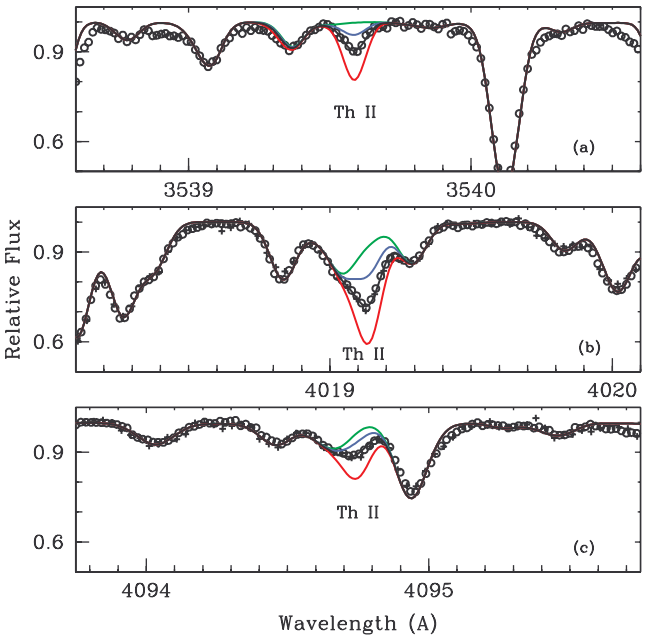

FIG. 7.—Observed and synthetic spectra of three Th II lines in HD 221170. All lines and symbols are as in Fig. 6.

Thorium ($Z = 90$, Th II).—Yushchenko et al. (2002) were the first to report on the abundance of Th in this star. In their expanded follow-up, Yushchenko et al. (2005) employed seven lines. Five of these lines ($\lambda\lambda$4019.1, 4086.5, 4094.7, 4179.7, and 5989.0) were included in the Nilsson et al. (2002) laboratory study of Th II, but the $\lambda\lambda$4003.3 and 4178.1 lines were not. Therefore, Yushchenko et al. (2005) quoted mean Th abundances both from the five lines with Nilsson et al. (2002) log *gf*-values and from the whole set of seven lines. Of their five lines with Nilsson et al. (2002) data, three must be viewed with caution. The λ4094.75 line is present in the HD 221170 spectrum, but it is blended with Er II λ4094.64, CH λ4094.70, and Fe II λ4094.73. The λ4179.71 line is intrinsically very weak, and it lies between (and is mostly masked by) Nd II λ4179.58 and Zr II λ4179.81. It is useful only to estimate an upper limit of the Th abundance. The λ5989.05 line occurs in a spectral region of significant telluric H_2O contamination, which must be removed from the HD 221170 spectrum via division by the spectrum of a rapidly rotating hot star.

In the present study we have chosen to consider only Th II lines with transition probabilities determined by Nilsson et al. (2002). Our search for lines in the HD 221170 spectrum yielded seven total, four in common with Yushchenko et al. (2005). In Figure 7 we show synthetic and observed spectra for three lines. Figure 7*a* displays an apparently clean feature at 3539.6 Å. We have discovered no plausible identification other than Th II at this wavelength. In Figure 7*b* we show the λ4019.1 line, which in previous studies often has served as the sole Th abundance indicator. This line appears to be relatively clean in extremely *r*-process–rich stars such as CS 31082−001 (see Fig. 9 of Hill et al. 2002). However, in higher metallicity, less extreme *r*-process stars, there are well-known blending issues that increase the Th abundance uncertainty from this complex blend. We have modeled the total feature as well as possible, trying to account for ^{13}CH, Ce II, Fe I, and Co I contaminants, but the resulting abundance here should be viewed with caution. Finally, in Figure 7*c*

we show the λ4094.7 line. The observed feature on our spectra clearly is a blended one, with an FWHM that is larger than any neighboring single line. This illustrates our contention that it is substantially more blended than is the λ4019.1 line. The Th abundance derived from this feature is very sensitive to the assumed strengths of the contaminating transitions listed in the preceding paragraph.

The final Th abundance is taken here as a straight mean of the results for all seven Th II transitions. There are various blending issues associated with most of these lines, and only the $\lambda\lambda$3539.6 and 4019.1 lines are strong enough to dominate the surrounding contaminants. But the synthetic/observed spectrum matches yield nearly the same abundance from all lines, lending confidence to the derived mean.

4. ABUNDANCE RESULTS

Table 1 includes the derived abundance for each feature, in $\log \epsilon(\mathrm{X})$ (col. [6]) and in bracket notation relative to the scaled solar value (col. [7]), where the abundance for individual lines is displayed. For iron, the bracket notation values are [Fe/H], and for all other elements X the values are [X/Fe]. In Table 3 we present a summary of the abundances derived from both EW measurements and spectrum syntheses. The first column denotes whether the abundance is from a neutral or ionized species, or if it represents the mean. The mean abundance was calculated by treating all lines of a given species with equal weight. The value of σ_{lines} denotes the σ derived from the line-to-line scatter. The value of $\sigma_{\mathrm{adopted}}$ includes an allowance for any uncertainty in the spectroscopically derived parameters. Abundances derived from a single feature have been assigned a minimum $\sigma = 0.2$ dex, and for species represented by only two lines, we have assigned a minimum $\sigma = 0.1$ dex.

For species represented by less than about five or fewer lines, uncertainties associated with individual transitions (blending, continuum placement, transition probabilities, hyperfine/isotopic substructure) are the limiting factors in the mean abundances.

As emphasized by the referee and noted by Erspamer & North (2003), continuum placement can be an unaccounted-for source of error in some abundance analyses. Erspamer & North (2003) find that continuum placement errors as small as 1% can have a large affect on the abundance results of some stars obtained from even high-S/N, high-resolution data such as those gathered with the ELODIE échelle spectrograph. Table 2 and Figure 3 of their study of A–F stars show that abundance differences of up to a few tenths of a dex can occur in stars possessing $V \sin i$ of 150 km s^{-1}. Fortunately, the $V \sin i$ of our K star HD 221170 is lower than the lowest $V \sin i$ value presented by Erspamer & North (2003), for which they determined that abundance differences resulting from systematic uncertainties in continuum placement of $\pm 1\%$ were all less than 0.1 dex. For species with more transitions, these concerns are of less importance; systematic effects (scale uncertainties in transition probabilities, model atmosphere parameter choices, etc.) begin to dominate.

To illustrate the line-to-line scatter for some of the *n*-capture elements in the HD 221170 spectrum, in Figure 8 we plot abundances from individual transitions as functions of wavelength, for six species with at least eight transitions apiece. The chosen species are Nd II, with the largest number of lines in our analysis; La II, Pr II, Tb II, and Ho II, rare earth elements whose abundances must be derived from synthetic spectra that take account of HFS; and Eu II, which has significant hyperfine and isotopic splitting as well. The number of lines and the standard deviations (σ) are noted in each panel of the figure. Several of these elements have useful lines spanning a large wavelength range ($\Delta\lambda \gtrsim 1000$ Å). However, Tb and Ho (Figs. 8*e* and 8*f*, respectively) have detectably strong transitions only at shorter wavelengths ($\lambda \lesssim 4000$ Å). It is clear from this figure that the derived abundances have no significant dependence on wavelength. The abundances also show no obvious variations correlated with line excitation potential or $\log gf$, but the baselines in those two quantities are too small to warrant further comment.

5. COMPARISON OF ABUNDANCE RESULTS WITH OTHER STUDIES

In this section we compare our derived abundances for HD 221170 with those obtained in other studies, as well as with the expectations from scaled solar *r*-process pattern predictions and with other *r*-process–rich stars.

5.1. *Comparison to Other Studies of HD 221170*

To date, the most comprehensive abundance studies of HD 221170 have been those of Yushchenko et al. (2002, 2005) and Gopka et al. (2004). Other abundance analyses have been made in the context of other programs, with usually only a limited set of elemental abundances investigated in a given study. Burris et al. (2000) analyzed HD 221170 using data of $R \simeq 20{,}000$ and a wavelength coverage of 4070 Å $< \lambda <$ 4710 Å, supplemented with data surrounding the Ba II λ6141 feature. For the seven elements of $Z > 39$ in common, we find $\langle \Delta[\mathrm{X/Fe}] \rangle_{\mathrm{Burris}} = -0.14$ ($\sigma = 0.13$), in the sense of this study minus Burris et al. (2000). Barklem et al. (2005) included HD 221170 as a comparison object (S/N $\sim$ 50) in their survey of *r*-process–enhanced stars taken with $R \sim 20{,}000$ and wavelength coverage of 3760 Å $< \lambda <$ 4980 Å. Comparing the same elemental range, for seven elements in common, we find $\langle \Delta[\mathrm{X/Fe}] \rangle_{\mathrm{Barklem}} = -0.10$ ($\sigma = 0.03$), in the sense of this study minus Barklem et al. (2005). Fulbright (2000) also observed this star. While we obtain excellent agreement with the EWs in common with the Fulbright study (recall Fig. 2), for the three elements of $Z > 39$ in common, we find $\langle \Delta[\mathrm{X/Fe}] \rangle = +0.25$ ($\sigma = 0.19$), where the abundance differences are driven by the large ξ_t (2.75 km s^{-1}) adopted by Fulbright. In addition, in the independent analysis by Simmerer et al. (2004) based on 2d-coudé data alone, a value of $\log \epsilon(\mathrm{Eu/La}) = -0.13$ was derived, the same value as derived in this study.

For the 35 elements in common with the Yushchenko et al. (2005) study, $\langle \Delta[\mathrm{X/Fe}] \rangle_{\mathrm{Yuschenko}} = +0.04$ ($\sigma = 0.19$), in the sense of this study minus Yushchenko et al. (2005). The mean difference between the two studies in a direct comparison of [X/Fe] values is statistically insignificant. This difference is fortuitously small, but it is also meaningless: the mean abundance difference encodes little or no information across 35 elements. The analysis of the derived abundances in HD 221170 involves careful comparisons against predicted abundance patterns. Patterns are examined in the deviations from the mean (σ). Deviations from the mean are of tremendous importance because those individual elements can be the basis from which critical inferences are made. Before confronting nucleosynthetic predictions, one requires a *reliable* set of derived abundances.

In Figure 9 we display the differences of the heavy *n*-capture abundances derived in this and the Yushchenko et al. (2005) studies with respect to the scaled solar *r*-process predictions of Simmerer et al. (2004).

As in our previous papers on *r*-process–rich stars, we have normalized the derived abundances to the value derived for $\log \epsilon(\mathrm{Eu})$ in the corresponding study. By most accounts, $\sim$95% of the Eu in the Sun was produced by the *r*-process: 93% (Käppeler et al. 1989), 94% (Arlandini et al. 1999; Travaglio

TABLE 3
HD 221170: Abundance Summary

Species	Z	$\log\epsilon(\mathrm{X})_\odot$	$\log\epsilon(\mathrm{X})_\star$	Error (±)	σ_{lines}	$\sigma_{\mathrm{adopted}}$	N	[X/Fe][a]
⟨C I⟩	6	8.56	5.67	...	...	0.30	CH	−0.71
⟨N I⟩	7	8.05	6.46	...	...	0.35	CN	+0.59
⟨O I⟩	8	8.93	6.97	0.00	0.00	0.10	2	+0.22
⟨Na I⟩	11	6.33	3.92	0.03	0.04	0.10	2	−0.23
⟨Mg I⟩	12	7.58	5.81	0.03	0.06	0.06	6	+0.41
⟨Si I⟩	14	7.55	5.85	0.05	0.09	0.09	4	+0.48
⟨Ca I⟩	20	6.36	4.53	0.02	0.09	0.09	15	+0.35
⟨Sc II⟩	21	3.10	1.01	0.02	0.06	0.06	9	+0.09
Ti I	...	...	3.04	0.03	0.12	0.12	13	+0.23
Ti II	...	...	3.16	0.03	0.11	0.11	15	+0.36
⟨Ti⟩	22	4.99	3.10	0.02	0.13	0.13	28	+0.30
V I	...	...	1.83	0.03	0.07	0.07	6	+0.01
V II	...	...	2.11	...	...	...	...	+0.01:UL
⟨V⟩	23	4.00	1.83	0.03	0.07	0.07	6	+0.01
Cr I	...	...	3.31	0.02	0.04	0.04	7	−0.18
Cr II	...	...	3.63	0.04	0.09	0.09	7	+0.15
⟨Cr⟩	24	5.67	3.47	0.05	0.18	0.18	14	−0.01
Mn I	...	...	2.91	0.04	0.10	0.10	6	−0.30
Mn II	...	...	3.19	...	...	...	...	−0.02:UL
⟨Mn⟩	25	5.39	2.91	0.04	0.10	0.10	6	−0.30
Fe I	...	...	5.34	0.01	0.12	0.12	157	−2.18
Fe II	...	...	5.32	0.02	0.10	0.10	19	−2.20
⟨Fe⟩	26	7.52	5.34	0.01	0.12	0.12	176	−2.18
⟨Co I⟩	27	4.92	2.87	0.04	0.12	0.12	9	+0.13
⟨Ni I⟩	28	6.25	4.16	0.05	0.13	0.13	6	+0.09
⟨Cu I⟩	29	4.21	1.27	...	...	0.20	1	−0.76
⟨Zn I⟩	30	4.60	2.51	0.00	0.00	0.10	2	+0.09
⟨Ga I⟩	31	2.88	0.59	...	...	0.20	1	−0.54
⟨Rb I⟩	37	2.60	0.70	...	...	0.30	1	+0.28
Sr I	...	...	0.48	...	...	0.20	1	−0.24
Sr II	...	...	0.85	0.04	0.08	0.08	4	+0.13
⟨Sr⟩	38	2.90	0.74	0.08	0.18	0.18	5	+0.02
⟨Y II⟩	39	2.24	−0.08	0.02	0.07	0.07	16	−0.13
Zr I	...	...	0.65	0.06	0.13	0.13	5	+0.23
Zr II	...	...	0.68	0.03	0.09	0.09	12	+0.26
⟨Zr⟩	40	2.60	0.67	0.02	0.10	0.10	17	+0.25
⟨Nb II⟩	41	1.42	−0.37	...	...	0.30	1	+0.39
⟨Mo I⟩	42	1.92	0.03	0.03	0.04	0.10	2	+0.29
⟨Ru I⟩	44	1.84	0.22	0.01	0.03	0.05	6	+0.56
⟨Rh I⟩	45	1.12	−0.35	0.13	0.23	0.23	3	+0.71
⟨Pd I⟩	46	1.69	−0.03	0.02	0.03	0.05	3	+0.46
⟨Ag I⟩	47	1.24	−0.50	0.05	0.07	0.10	2	+0.44
⟨Sn I⟩	50	2.00	−0.40	...	...	...	...	−0.22:UL
⟨Ba II⟩	56	2.13	0.21	0.04	0.12	0.12	8	+0.26
⟨La II⟩	57	1.14	−0.73	0.01	0.06	0.06	36	+0.32
⟨Ce II⟩	58	1.55	−0.41	0.02	0.12	0.12	44	+0.22
⟨Pr II⟩	59	0.71	−1.04	0.01	0.06	0.06	21	+0.43
⟨Nd II⟩	60	1.45	−0.35	0.01	0.08	0.08	63	+0.39
⟨Sm II⟩	62	1.00	−0.66	0.01	0.07	0.07	28	+0.52
⟨Eu II⟩	63	0.51	−0.86	0.02	0.07	0.07	16	+0.80
⟨Gd II⟩	64	1.12	−0.46	0.04	0.14	0.14	11	+0.60
⟨Tb II⟩	65	0.28	−1.21	0.03	0.08	0.08	8	+0.69
⟨Dy II⟩	66	1.10	−0.32	0.02	0.07	0.07	14	+0.76
⟨Ho II⟩	67	0.51	−0.97	0.02	0.07	0.07	8	+0.70
⟨Er II⟩	68	0.93	−0.48	0.06	0.13	0.13	4	+0.77
⟨Tm II⟩	69	0.13	−1.38	0.02	0.06	0.06	6	+0.68
⟨Yb II⟩	70	1.08	−0.51	...	...	0.20	1	+0.59
⟨Lu II⟩	71	0.12	−1.40	...	...	...	...	+0.66:UL
⟨Hf II⟩	72	0.88	−0.94	0.02	0.04	0.04	5	+0.47
⟨W I⟩	74	0.68	−0.60	...	...	...	...	+0.90:UL
⟨Os I⟩	76	1.45	0.16	0.04	0.10	0.10	7	+0.90
⟨Ir I⟩	77	1.35	0.02	0.09	0.13	0.13	2	+0.85
⟨Pb I⟩	82	1.85	−0.09	0.15	0.21	0.21	2	+0.24
⟨Th II⟩	90	0.12	−1.46	0.02	0.05	0.05	7	+0.60

[a] The abundances of individual ions relative to the scaled solar value: [Fe I/H], [Fe II/H], or [X/⟨Fe⟩] for $\langle[\mathrm{Fe/H}]\rangle = -2.18$. Upper limits are denoted :UL.

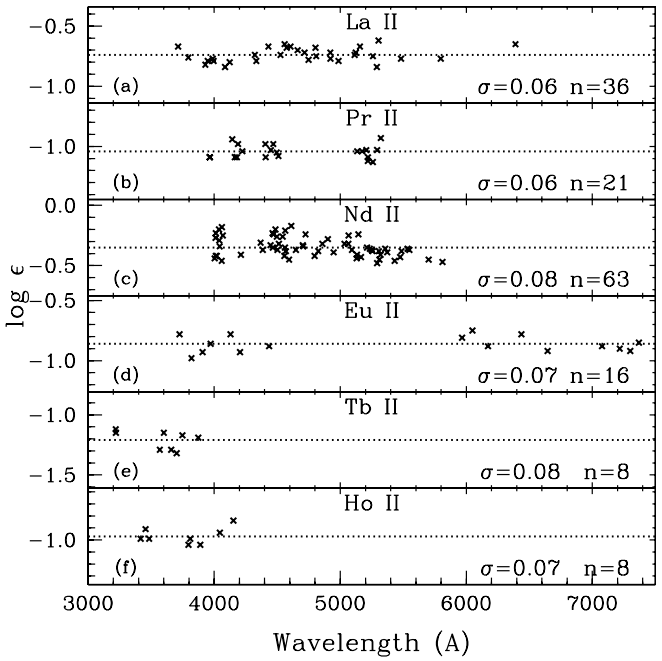

FIG. 8.—Abundances from individual lines of six rare earth element species, plotted against line wavelengths. The mean abundances are indicated by dotted horizontal lines, with the scatter about the mean (σ) and the number of lines employed (n) stated in each panel.

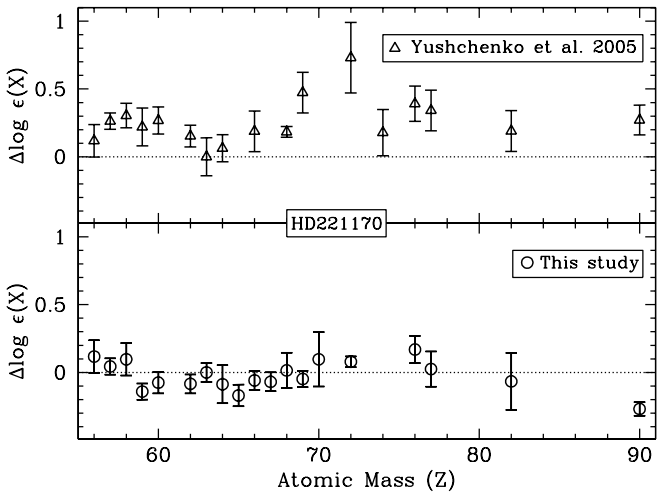

FIG. 9.—HD 221170 abundance comparisons of the heavy n-capture elements to the predicted scaled solar r-process pattern of Simmerer et al. (2004). *Top:* Difference in the abundances reported by Yushchenko et al. (2005). *Bottom:* Differences derived in this study. The derived abundances have been normalized to the value derived for $\log \epsilon$(Eu) in the corresponding study. The error bars displayed are those of the $1 - \sigma_{\rm adopted}$ values.

et al. 2004), 97% (Burris et al. 2000; as also reported in Simmerer et al. 2004).

As Yushchenko et al. (2005) note, their derived n-capture abundance pattern for HD 221170 normalized to Er does not match well the scaled solar r-process abundance distribution, particularly for elements with $Z > 68$. In addition to the difficulties of analyzing Er (see § 3.4), there are other potential pitfalls in normalizing to Er. Only ~85% of the solar Er is produced via the r-process (see references given in § 1). The r-process contribution to Er less resembles Eu, Ir, Pt, and Au than it does Bi, Gd, Tm, and Dy. In studies of metal-poor stars with $s + r$ enhancements (see, e.g., Aoki et al. 2002; Johnson & Bolte 2004), [Er/Eu] can be ~1 *regardless* of whether or not the stars possess strong r-process enhancements.

In Figure 9, the derived abundances of both studies have both been normalized to the value derived for $\log \epsilon$(Eu) in the corresponding study. In contrast to the results of Yushchenko et al. (2005), in this atomic mass range, we find good agreement between the abundances derived here and the predicted scaled solar r-process values. Our derived Th abundance is discussed further in § 7. For some other elements, there is a disagreement between the derived solar photospheric and chondritic/meteoritic abundances. For instance, Lodders (2003) notes discrepancies of −0.07, +0.11, and +0.08 dex for Pr ($Z = 59$), Hf ($Z = 72$), and Os ($Z = 76$), respectively. Incorporating additional uncertainties such as these in the *solar* abundance scale is sufficient to push our observed and predicted abundances into good agreement.

Many of the abundance differences between our results and those of Yushchenko et al. (2005) appear to arise from differences in the quality of the spectra employed in the two studies. Some of the most obvious differences can be detected by eye. For instance, a comparison can be made between the spectra displayed in the panels of our Figure 1 and the spectra shown in Figure 2 of Yushchenko et al. (2002) and Figures 1–4 of Yushchenko et al. (2005). As already noted in § 2, the appearance of the spectra employed by Yushchenko et al. (2002, 2005) is quite different from either the Keck HIRES or McDonald 2d-coudé data employed here. Furthermore, as shown in our Figure 2, there are significant differences in the EWs measured by Yushchenko et al. (2005), against not only those of this study measured in Keck HIRES and McDonald 2d-coudé data, but also those of yet another independent set of measurements employing Lick Hamilton data (Fulbright 2000). In addition, there are differences in the atomic parameters employed in the two studies (e.g., for elements such as Sm, Nd, Eu, and Th). The thorium abundance differences, in particular, seem to relate not only to differences in the adopted $\log gf$-values, but we note that the differences are a function of wavelength, increasing redward. We suggest that the thorium abundance differences may be more related to line strengths and data quality than to anything else. Furthermore, in many cases, the lines employed in the Yushchenko et al. (2005) study yielded anomalously large abundances due to unaccounted-for blends, including but not limited to those arising from HFS splitting. Thus, we are unable to replicate many of the n-capture abundances deduced by Yushchenko et al. (2005) for HD 221170.

5.2. *Comparison to Scaled Solar r-Process Predictions for $Z \geq 56$*

In Figure 10 we display the abundances we derived for HD 221170 in the context of predictions of the scaled solar r-process abundances by Simmerer et al. (2004) and Arlandini et al. (1999; with most values taken from Table 10 of Simmerer et al. 2004). In the study of BD +17 3248 by Cowan et al. (2002), it was found that the Arlandini et al. (1999) distribution seemed to fit the abundances of the r-process–rich star better than the predictions of Burris et al. (2000). Simmerer et al. (2004) slightly revised the Burris et al. (2000) values and included the updated value of La from O'Brien et al. (2003), which they also incorporated in their updated Arlandini et al. (1999) La value. Furthermore, we take into account here the r-only isotopic contributions of ^{124}Sn, ^{130}Te, ^{136}Xe, and ^{150}Nd to the total scaled solar $1 - s = r$-process abundance predictions to the Arlandini et al. (1999) values presented in Simmerer et al. (2004). The resulting predictions are labeled Arlandini* and are those employed for the remainder of this paper.

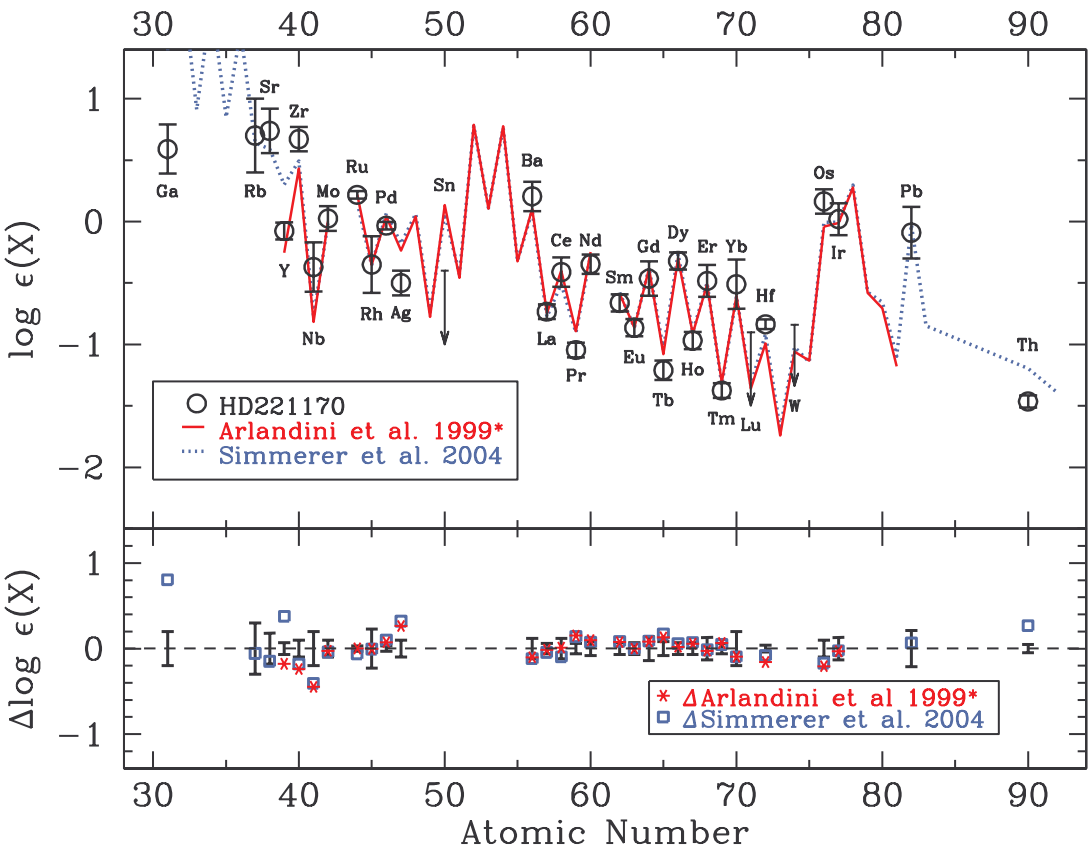

FIG. 10.—Comparison of the $\log \epsilon(X)$ abundances for $Z > 30$ in HD 221170 with the scaled solar *r*-process predictions from Simmerer et al. (2004; *solid red line*) and those based on Arlandini* (largely 1999; with modifications as described in § 5.2; *dotted blue line*). Both sets of predictions have been normalized to the value derived for $\log \epsilon(Eu)$ in HD 221170. In the top panel, the upper limits and open circles with error bars denote the stellar abundances. The bottom panel displays the difference defined as $\Delta \log \epsilon(X) \equiv \log \epsilon(X)_{pred} - \log \epsilon(X)_{obs}$, where the error bars are those we adopted for the abundances derived for each element. Upper limits are not displayed in the bottom panel.

For 13 elements with $56 \leq Z \leq 69$ in BD +17 3248, the differences between the observed abundances and the scaled solar predictions normalized to the Eu abundance value derived for BD +17 3248 [$\Delta \log \epsilon(X) \equiv \log \epsilon(X)_{pred} - \log \epsilon(X)_{obs}$] are $\langle \Delta(\log \epsilon) \rangle_{Arlandini^*} = 0.031 \pm 0.019$ ($\sigma = 0.068$) versus $\langle \Delta(\log \epsilon) \rangle_{Simmerer} = 0.038 \pm 0.024$ ($\sigma = 0.081$). For the same elemental range, we obtain the following differences in the abundances of HD 221170 and the predictions of the scaled solar *r*-process pattern, normalized to our Eu abundance: $\langle \Delta(\log \epsilon) \rangle_{Arlandini^*} = -0.042 \pm 0.019$ ($\sigma = 0.070$) and $\langle \Delta(\log \epsilon) \rangle_{Simmerer} = -0.035 \pm 0.024$ ($\sigma = 0.086$). Thus, in the case of HD 221170, the scatter is slightly smaller with respect to the Arlandini* scaled solar *r*-process abundances, with the offset slightly smaller with respect to the Simmerer et al. (2004) predictions. The differences are small but not a function of metallicity: within the uncertainty, both stars share the same metallicity ([Fe/H] of BD +17 3248 is −2.08 with $\sigma = 0.08$, and that of HD 221170 is −2.18 with $\sigma = 0.12$).

6. REVISITING THE ISSUE OF MULTIPLE *r*-PROCESS SITES

In Figure 11 we overplot the Simmerer et al. (2004) scaled solar *r*-process predictions along with the abundances of HD 221170 and other *r*-process–rich stars: CS 22892−052 (Sneden et al. 2003), HD 115444 (Westin et al. 2000), and BD +17 3248 (Cowan et al. 2002). Abundance studies of the ultra–*r*-process–rich metal-poor star CS 22892−052 have shown that, while the abundances of $Z \geq 56$ seem to match well the predictions from the scaled solar *r*-process, the lighter elements in the range of $40 < Z < 56$ are underabundant (Sneden et al. 2003). In general, the agreement in the abundance distribution patterns of the heavy *n*-capture elements ($Z \geq 56$) in these *r*-process–rich stars suggests that a robust and perhaps even unique *r*-process produced these elements. However, the same does not appear to be true of the lighter *n*-capture elements.

Observationally, many of the light *n*-capture elements are challenging to detect, requiring space-based observations. With the aid of the Space Telescope Imaging Spectrograph (STIS) on the *Hubble Space Telescope* (*HST*), Cowan et al. (2005) derived abundances of Ge, Zr, Os, and Pt in a sample of metal-poor stars, including HD 221170. As noted in § 3.3, the spectrum of HD 221170 is complex, and more so in the blue–violet–UV regions than in the green–yellow–red. Despite the difficulties, their results for the abundances in common with this study are within the stated errors.

The differences in the light versus heavy *n*-capture elemental abundance patterns are not restricted to observations of metal-poor halo stars. In an investigation of the abundances of short-lived isotopes in the early solar system (as inferred from meteoritic analyses) Wasserburg et al. (1996) found that distinctive SN sources or *r*-process sites were required to explain the incompatibility in the observed $^{129}I/^{182}Hf$ ratio. Both isotopes are short lived and essentially of *r*-process origin, thus inferring two distinct *r*-process sites for the light isotopes below Ba and for the heavy isotopes beyond Ba. Their model of "uniform production" produced abundances that match those of actinides and the short-lived

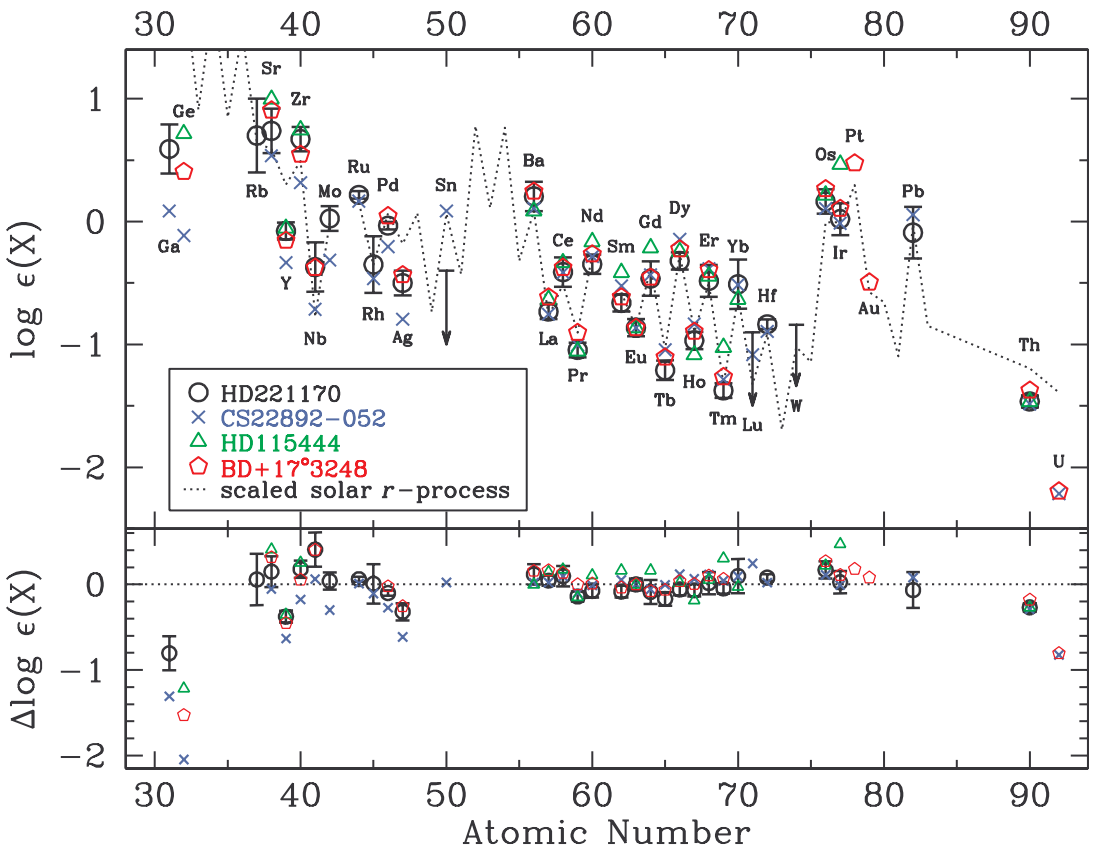

FIG. 11.—Comparison of the $\log \epsilon(X)$ abundances of $Z > 30$ in HD 221170 with those of CS 22892−052 (*blue crosses*; Sneden et al. 2003, including upper limits for Ga, Ge, Sn, and U), HD 115444 (*green triangles*; Westin et al. 2000), BD +17 3248 (*red pentagons*; Cowan et al. 2002), and the predicted scaled solar *r*-process pattern (*dotted line*; Simmerer et al. 2004). Both the derived and predicted abundances have been normalized to the value derived for $\log \epsilon(\mathrm{Eu})$ in HD 221170. To lessen confusion, upper limits are indicated only for HD 221170. The bottom panel displays the difference defined as $\Delta \log \epsilon(X) \equiv \log \epsilon(X)_{\mathrm{obs}} - \log \epsilon(X)_{\mathrm{pred}}$ for all four *r*-process–rich stars with respect to the scaled solar *r*-process predictions of Simmerer et al. (2004).

^{182}Hf but overproduced the abundances of the lighter isotopes. This suggested to Wasserburg et al. (1996) that multiple *r*-process sites were required to produce both the heavy and light isotopes. In another study of the short-lived radioactive isotopes in the early solar system, Meyer & Clayton (2000) found that the abundances of the lighter isotopes *could* be explained by continuous galactic nucleosynthesis (providing a match to the inferred abundance of ^{129}I, among other isotopes) combined with a relatively more recent injection of material into the condensing protosolar nebula (providing a source for the relatively enhanced abundance of ^{182}Hf, as well as ^{26}Al, ^{36}Cl, ^{41}Ca, and ^{60}Fe). The ^{182}Hf site suggested by Meyer & Clayton (2000) is a "fast *s*-process" (with special conditions surrounding the subsequent mass lost from the progenitor star) rather than in the *r*-process proper. Production of ^{182}Hf is essentially driven by neutron captures in the outer He shell region by explosive nucleosynthesis (Meyer 2005). The Meyer & Clayton (2000) model is reminiscent of a model discussed by Cameron et al. (1993), who also invoked *s*-processing to explain some of the inferred abundances of isotopes normally considered to be of primarily *r*-process origins in the early solar system.

Although the Cameron et al. (1993), Wasserburg et al. (1996), and Meyer & Clayton (2000) studies disagree as to the proportions of "uniform" or "continuous" production required to explain the inferred meteoritic abundance patterns of the short-lived isotopes in the early solar system, all of the studies invoke another source, beyond continuous Galactic *r*-process production, to explain the discrepant abundances of isotopes normally considered to be of primarily *r*-process origin. For further discussion of this issue, we refer the reader to Goswami et al. (2005) and Wasserburg et al. (2006) for recent reviews.

A phenomenological model for the formation of the *n*-capture abundance patterns observed in *r*-process–rich metal-poor stars has been developed by Qian & Wasserburg (2000) and Wasserburg & Qian (2000). The model replicates many of the observed abundance patterns in very metal-poor stars with a mix of two different types of *r*-process events that occur on different frequencies (high and low) and produce different sets of yields (heavy and light *n*-capture elements). Another point of view taken to explain the light versus heavy *n*-capture abundance patterns has been to postulate the existence of both a "main" and a "weak" *r*-process. The main *r*-process would produce the (underabundant light) *n*-capture abundance patterns observed in the low-metallicity *r*-process–rich stars. A weak *r*-process, presumed to be a secondary process (i.e., dependent on an existing heavy-element distribution) and possibly the result of only a small neutron burst, would then operate on existing seeds to produce the observed solar abundance pattern in the light *n*-capture elements (see, e.g., Pfeiffer et al. 2001; Thielemann et al. 2001; Truran et al. 2001). Both of these views have been developed in response to the different abundance pattern characteristics between the light and heavy *n*-capture elements.

As shown in Figures 9–11, the abundances of the heavy *n*-capture elements derived in this study are well matched by the scaled solar *r*-process pattern predictions. Surprisingly, the abundances of HD 221170 also seem to be a better match to the scaled solar *r*-process predictions in the $37 < Z < 48$ elemental range than those of other *r*-process–rich stars. Figure 12 takes a closer

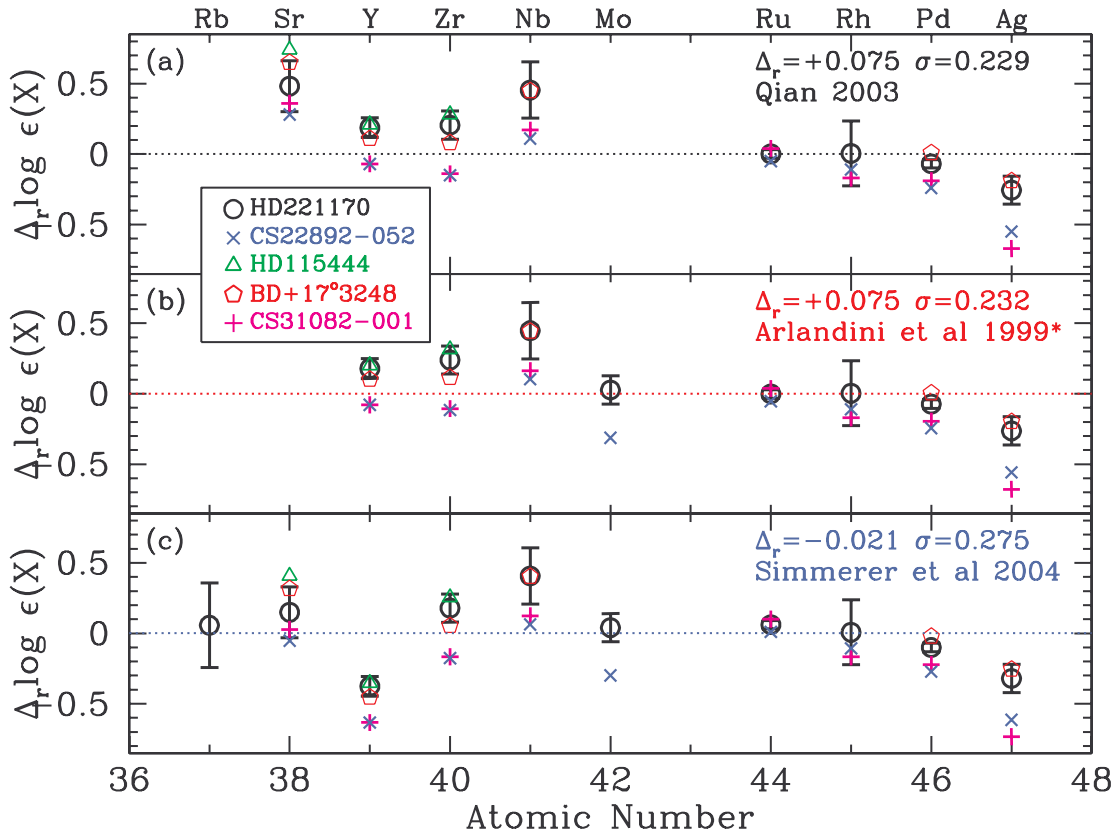

FIG. 12.—Comparison of the abundances of $37 \leq Z < 50$ in HD 221170 with those of CS 22892−052, HD 115444, BD +17 3248, and the scaled solar *r*-process predictions, with symbols and normalization as described in Fig. 11. Here we also add the results for CS 31082−001 (*magenta plus signs*; Hill et al. 2002). The three panels display the difference $[\Delta \log \epsilon(\mathrm{X}) \equiv \log \epsilon(\mathrm{X})_{\mathrm{obs}} - \log \epsilon(\mathrm{X})_{\mathrm{pred}} = \Delta_r]$ and scatter (σ) for all five *r*-process–rich stars with respect to the scaled solar *r*-process predictions of Qian (2003), Arlandini* (largely 1999; with modifications described in § 5.2), and Simmerer et al. (2004).

perspective on this issue. We display the abundance differences with respect to three predictions of the scaled solar *r*-process pattern: those of Qian (2003), Arlandini* (largely 1999; with modifications as described in § 5.2), and Simmerer et al. (2004). The individual panels show the value of $\langle \Delta(\log \epsilon) \rangle$ and σ for the elements in common. In addition to the *r*-process–rich stars shown in the previous figures, we have included here the abundances of CS 31082−001 (Hill et al. 2002). Regardless of whose scaled solar *r*-process predictions are referenced, the abundance patterns of *r*-process–rich stars in this light *n*-capture elemental range appear to have been stamped from a similar mold, but with an offset in the overall abundances.

In these *r*-process–rich metal-poor stars, it would appear that at least some of the light *n*-capture elements arise in sites that produce similar abundance yields, but with overall amounts that do not scale with the predicted scaled solar *r*-process values. Too little information exists in the literature regarding the abundance of Ga ($Z = 31$) in metal-poor stars to warrant any comment beyond urging observers to obtain abundances of this element. However, in the case of Ge ($Z = 32$), Cowan et al. (2005) have shown that the abundance of [Ge/H] seems to track well the abundance of [Fe/H], whereas [Ge/Fe] appears to be independent of the [Eu/Fe] ratio. The behavior of [Zr/Fe], on the other hand, is qualitatively different. As can be seen in Figure 10 of the extensive investigation of Sr, Y, and Zr by Travaglio et al. (2004), [Zr/Fe] has only a mild dependence on the abundance of [Fe/H]. However, the largest [Zr/Fe] abundance displayed by Cowan et al. (2005, their Fig. 6) corresponds to the star with the largest [Eu/Fe] abundance, CS 22892−052. Regarding other elements in this atomic mass range, the abundances of Pd and Ag have not been reported for HD 115444, nor have Mo, Ru, and Rh for either it or BD +17 3248.

Iron peak and transiron isotopes can be produced in the neutron-rich α-rich freezeout process. Such high-entropy environments, such as those of nascent neutron stars, possess excess neutron and α-particle distributions that can lead to the production of iron peak isotopes, particularly those to the high-Z side of the iron peak (see, e.g., Arnett et al. 1971; Woosley & Hoffman 1992; Nakamura et al. 1999). This process is not necessarily coupled to the *n*-capture nucleosynthesis of higher atomic mass isotopes. Thus, it has been suggested that the α-rich freezeout process may be responsible for the behavior of Ge abundances with metallicity (Cowan et al. 2005). Furthermore, the α-rich freezeout process has been invoked as a possible explanation for the overabundance of Sr (McWilliam & Searle 1999) and Y (Venn et al. 2004) observed in some metal-poor halo stars. In the case of HD 221170, however, a boost from an overall increase in the efficiency of the α-rich freezeout does not successfully explain its light *n*-capture abundance pattern. The abundances of lighter transiron elements (and sensitive to the neutron excess and the entropy; see, e.g., Arnett et al. 1971), such as Cu ($Z = 29$), Zn ($Z = 30$), and Ge ($Z = 32$), all have values in HD 221170 that are in accord with those derived for BD +17 3248, HD 115444, and CS 22892−052. Thus, the abundances of the elements in HD 221170 in the range of $28 < Z \leq 32$ do not seem to support an α-rich freezeout explanation for the overall relative enhancement in HD 221170 of the abundances of elements in the range of $37 < Z < 48$. We refer the reader to Bisterzo et al. (2004) for more extensive discussions regarding the

complex origins of Cu and Zn, and to Travaglio et al. (2004) for Sr, Y, and Zr.

The understudied abundances in the atomic mass range between the iron peak and $Z < 56$ present a shopping list of elements that need to be examined and reported for a larger sample of metal-poor stars. Interestingly, while we can only report an upper limit for the abundance of Sn in HD 221170, the value is significantly lower than the predicted scaled solar value. While some light *n*-capture elements with features only in the UV wavelengths are limited to satellite observations, the near-UV–sensitive detector on the Keck HIRES places at least some of the understudied elements within the reach of a ground-based facility (see Table 1).

7. NUCLEOCOSMOCHRONOMETRY OF HD 221170 AND OTHER *r*-PROCESS–RICH STARS

With its very long half-life, the detection of Th in HD 221170 allows for nucleocosmochronometric estimates for the age of this star. The ideal chronometer pair for these age determinations is Th/U, since both elements are made entirely in the *r*-process and are nearby in mass number (see discussions in the reviews of Truran et al. 2002; Sneden & Cowan 2003; Cowan & Sneden 2004; Cowan & Thielemann 2004). Th/U has been used to determine the ages of CS 31082−001 (12.5 ± 3 Gyr, Cayrel et al. 2001; 14 ± 2.4 Gyr, Hill et al. 2002; 15.5 ± 3.2 Gyr, Schatz et al. 2002; 14.1 ± 2.5 Gyr, Wanajo et al. 2002) and BD +17 3248 (13.8 ± 4 Gyr; Cowan et al. 2002). However, uranium (with its inherently low abundance and frequent spectral blending with strong atomic and molecular features) is difficult to detect in most stars and was not seen in HD 221170.

Chronometric age estimates based on the Th/Eu ratio have been made for a number of stars (see, e.g., Sneden et al. 1996, 2000a, 2003; Cowan et al. 1997, 1999; Pfeiffer et al. 1997; Westin et al. 2000; Johnson & Bolte 2001; del Peloso et al. 2005). Our abundance determinations for HD 221170 indicate a ratio of $\log\epsilon(\mathrm{Th/Eu}) = -0.60$ with a typical observational uncertainty of $\sigma(\log\epsilon) = 0.05$. This ratio is virtually identical to that found for CS 22892−052 (−0.62; Sneden et al. 2003), BD +17 3248 (−0.51; Cowan et al. 2002), and HD 115444 (−0.60; Westin et al. 2000). The abundance ratio for HD 221170 is also consistent with the average $\log\epsilon$(Th/Eu) ratio found in two giant stars in the globular cluster M15 ($\langle -0.62\rangle$; Sneden et al. 2000b).

As indicated earlier in this paper, our abundance results do not agree with those of Yushchenko et al. (2005): we do not find an enhanced abundance of Th in HD 221170, and the (stable) *n*-capture elemental abundances in this star are consistent with the predicted scaled solar system *r*-process abundance distribution pattern and with other *r*-process–rich stars (e.g., CS 22892−052, BD +17 3248, CS 31082−01). Thus, in contrast to the suggestion of Yushchenko et al. (2005), we find that the abundance ratio of Th/Eu is indeed usable as a chronometer in this star.

Chronometric age estimates depend sensitively on the initial predicted values of Th/Eu, which in turn depend on the nuclear mass formulae and *r*-process models employed in making those determinations (see discussion in Schatz et al. 2002; Cowan & Sneden 2004). Calculations of the *r*-process are designed to replicate the solar system isotopic (and elemental) abundance distribution. The same calculations that reproduce the stable solar system (and stellar) elemental abundances are then used to predict the radioactive abundances and thus the Th/Eu ratio. Comparing the observed Th/Eu abundance (0.25) in HD 221170 with the predicted *r*-process values can directly yield an age determination via the following relation:

$$\left(\frac{\mathrm{Th}}{\mathrm{Eu}}\right)_{\star} = \left(\frac{\mathrm{Th}}{\mathrm{Eu}}\right)_{r} \exp\left(-\frac{t}{\tau_{\mathrm{Th}}}\right), \quad (1)$$

where τ_{Th} represents the characteristic decay timescale of Th (20.27 Gyr) and t the inferred age.

Earlier theoretical calculations predicted an initial value of Th/Eu = 0.48 in an *r*-process site (Cowan et al. 1999), while more recent calculations, constrained by some recent experimental data, suggest a value of 0.42 (Sneden et al. 2003). Kratz et al. (2004) find Th/Eu = 0.42 for traditional (i.e., "iron seed") calculations and a value of 0.48 for conditions that might be more typical of the high-entropy wind scenario in an SN II. Employing an average of these two initial abundance predictions for Th/Eu suggests an age for HD 221170 of 11.7 ± 1.4 Gyr. The error uncertainty here is strictly from the two different theoretical calculations. Observational abundance errors (e.g., $\log\epsilon = 0.05$) would also contribute to the general age uncertainty. Since these errors are uncorrelated, our best age estimate for HD 221170, based on the Th/Eu chronometer, is 11.7 ± 2.8 Gyr.

If we put aside the theoretical considerations for a moment and assume the Anders & Grevesse (1989) value of Th/Eu = 0.463 in the early solar system, then for the Th/Eu of 0.2512 ± 0.05 in HD 221170, we can use this information to derive an inferred age based on the adopted Th/Eu in the early solar system. Employing equation (1) [$0.25 \pm 0.05 = 0.463 \exp(-t/20.27\ \mathrm{Gyr})$], the inferred age is $12.4^{+4.5}_{-3.7}$ Gyr, in agreement with that derived employing the theoretical *r*-process calculations.

The age we derive for HD 221170 is within the range of cosmic ages determined by the results of the *Wilkinson Microwave Anisotropy Probe* (*WMAP*) experiment, both those combined with results from the Sloan Digital Sky Survey ($14.1^{+1.0}_{-1.9}$ Gyr; Tegmark et al. 2004) and those combined with earlier cosmic microwave background (CMB) and large-scale structure data (13.7 ± 0.2 Gyr; Spergel et al. 2003). These ages are also in agreement with the main-sequence turnoff ages of the oldest globular clusters ($12.5^{+3.5}_{-2.4}$ Gyr; Krauss & Chaboyer 2003; further refined to $12.6^{+3.4}_{-2.2}$ Gyr with the inclusion of CMB data; Jimenez et al. 2003). In turn, the white dwarf cooling curve age of 12.1 ± 0.9 Gyr, derived for globular cluster M4 (NGC 6121) by Hansen et al. (2004), is consistent with ages derived from the main-sequence turnoff for this cluster.

Although our age estimate for HD 221170 is consistent with those reported for *r*-process–rich stars, additional experimental and theoretical studies, particularly of very neutron-rich nuclei, are required to reduce meaningfully the chronometric age uncertainties. In particular, employing certain other nuclear mass formulae would lead to a wider range of initial abundance ratios and correspondingly wider range in age estimates. We note, however, that some of the mass models that have been employed to predict (wide ranging) initial chronometric age abundances do not reproduce the solar Pb and Bi abundances or adequately predict the nuclear properties of nuclei far from stability (see Cowan et al. 1999; Schatz et al. 2002).

The *r*-process–rich star CS 31082−001 is one well-documented case in which Th/Eu is anomalously high. While the abundances of the stable elements (through the third *r*-process peak) in CS 31082−001 are consistent with the predicted scaled solar system *r*-process distribution, Th and U are enhanced with respect to the

other *n*-capture elements (Hill et al. 2002; Schatz et al. 2002). Thus, in this star the Th/Eu chronometer leads to unreasonably low age determinations, while the Th/U ratio predicts an age consistent with other ultra–metal-poor halo stars. We note, however, that the reported lead abundance in CS 31082−001 (Plez et al. 2004), which predominantly results from α-decay of Th and U isotopes, seems to be too low with respect to such high abundance values of these radioactive elements (Kratz et al. 2004). Qian & Wasserburg (2001) have suggested that the U in CS 31082−001, along with the enhanced abundances of Os and Ir, may be the result of contamination from a nearby SN II event, sufficiently nearby to have come from a binary companion. If the binary companion survived, it likely became a stellar-mass black hole. Schlegel (2003) undertook a survey of all available X-ray data acquired in the vicinity of CS 31082−001. Observations by the *ROSAT* All-Sky Survey (Voges et al. 1999) set an upper limit on the X-ray luminosity that falls short of the expected flux emanating from the region surrounding a stellar-mass black hole at the assumed distance of CS 31082−001. However, *XMM-Newton* observations have been undertaken to uncover lower X-ray fluxes that are possibly being emanated from the system.

Models of SN II explosions have found that *r*-process nucleosynthesis can take place in the wind generated by neutrinos flowing outward from the surface of a hot newborn neutron star (see references given in § 1, as well as Otsuki et al. 2000 and additional references therein). Sasaqui et al. (2005) have investigated the effect that a sudden cessation of neutrino fluxes (resulting from the creation of a black hole) can have on the *r*-process nucleosynthesis yields. They find that not only are the resulting yields quite sensitive to the neutrino cutoff effect in their model, but also that the largest impact is on the abundance of the Th and U isotopes. In the case of CS 31082−001, their model with no *r*-process cutoff (and, by implication, no cessation of the neutrino fluxes through the formation of a black hole) provides the best match to the observations of Th and U.

Clearly, additional observational and theoretical studies of this star and others with enhanced actinide abundances, such as the recently discovered *r*-process–rich, Th-rich star CS 30306−132 (Honda et al. 2004), will be needed to better understand and further refine the chronometric age determinations.

8. SUMMARY AND CONCLUSIONS

Employing high-resolution data acquired with the Keck Observatory HIRES and supplemented by high-resolution data gathered with the McDonald Observatory 2d-coudé spectrograph, we have derived the abundances of 57 species in the metal-poor red giant star HD 221170. The stellar atmospheres have been derived employing spectroscopic constraints, eliminating abundance trends with the excitation potentials, EWs, and ionization states of ~200 iron peak lines, and are in good agreement with the $T_{\rm eff}$ and log g expectations based on photometric and parallax measurements.

In the abundance analysis, single-source and recent gf-values were employed wherever possible in order to diminish uncertainties resulting from systematics in combining multiple sources. Single, unblended features were analyzed using EWs, and more complex features synthesized, with HFS and isotopic splitting accounted for where necessary. In total, over 700 features were analyzed in this star, with the majority arising from *n*-capture transitions. Nearly all of the strongest *n*-capture transitions occur in the complex blue–UV spectral regions where blended features are the rule, not the exception. Therefore, we employed full synthetic spectrum analyses of more than half of the *n*-capture features we investigated. Included in our analysis are numerous *n*-capture features with newly determined atomic parameters. We provide improved wavelengths and full hyperfine and isotopic patterns for 24 lines of Eu II and complete hyperfine patterns for 80 lines of La II. More than 350 transitions of 35 species yielded abundances for 30 *n*-capture elements and significant upper limits for three others.

The resulting *n*-capture abundance pattern distribution for $Z \geq 56$ is fitted well by the predicted scaled solar system *r*-process abundances, as has been seen in other *r*-process–rich stars such as CS 22892−052, BD +17 3248, and HD 115444. We derive ratios of log ϵ(Th/La) = −0.73 (σ = 0.06) and log ϵ(Th/Eu) = −0.60 (σ = 0.05), values in excellent agreement with those previously derived for other *r*-process–rich metal-poor stars, including the giant stars of globular cluster M15. Also comparable is the inferred age, based on the Th/Eu chronometer, of 11.7 ± 2.8 Gyr (which includes the estimated uncertainty arising from both the measured abundances and the predicted Th/Eu production ratio), in accord with the cosmic age derived from the measurements made by *WMAP*. Thus, the abundance ratio of Th/Eu is indeed usable as a chronometer in this star.

Surprisingly, in contrast to the abundance patterns of other *r*-process–rich metal-poor stars, the abundances of HD 221170 also seem to be a better match to the scaled solar *r*-process predictions in the lighter *n*-capture element range of $37 < Z < 48$. Based on the abundances of iron peak and the lighter transiron elements, however, the source of the light *n*-capture agreement in HD 221170 does not appear to lie in the abundance predictions from the neutron-rich α-rich freezeout process.

The successful efforts by the HIRES CCD upgrade group are acknowledged, as is the expertise of the Keck staff during the run. We are grateful for the privilege to observe on the revered summit of Mauna Kea. I. I. I. is indebted to John Norris and Sean Ryan for their guidance on FIGARO/IRAF échelle reductions; to Andy McWilliam, Iván Ramírez, and Jorge Meléndez for supplying software tools; to Jon Fulbright and Andy McWilliam for sending line lists in electronic form; to Norbert Christlieb for sending results in electronic form; to George Preston, Yong-Zhong Qian, Jim Truran, Gerry Wasserburg, and Dave Yong for illuminating discussions; to Wako Aoki, Bob Kraft, and Alexander Yushchenko for their careful reading of (and helpful comments on) an earlier version of this paper; and to the reviewers for useful suggestions incorporated into the manuscript.

This research was supported via funding to I. I. I. through a Carnegie-Princeton Fellowship and from NASA through Hubble Fellowship grant HST-HF-01151.01-A from the Space Telescope Science Institute, operated by AURA, Inc., under NASA contract NAS5-26555; from the NSF through grants AST 03-07495 to C. S., AST 05-06324 to J. E. L., and AST 03-07279 to J. J. C.; and from the Italian MIUR-FIRB Project "The Astrophysical Origin of the Heavy Elements beyond Fe" to R. G. and S. B. We appreciate the use of NASA's Astrophysics Data System Bibliographic Services; the Database on Rare Earths at Mons University; the SIMBAD database, operated at CDS, Strasbourg, France; data products from the Two Micron All Sky Survey, which is a joint project of the University of Massachusetts and the Infrared Processing and Analysis Center/California Institute of Technology, funded by NASA and the NSF; and the NASA/IPAC Extragalactic Database (NED), which is operated by the Jet Propulsion Laboratory, California Institute of Technology, under contract with NASA.

TABLE 4
Isotopic Hyperfine Structure Patterns: ^{139}La

Wavenumber (cm^{-1})	λ (Å)	F_{upper}	F_{lower}	Component Position (cm^{-1})	Component Position (Å)	Strength
27549.30.....	3628.822	7.5	6.5	0.02310	−0.003043	0.22222
27549.30.....	3628.822	6.5	6.5	−0.00840	0.001106	0.02618
27549.30.....	3628.822	6.5	5.5	0.01396	−0.001839	0.16827
27549.30.....	3628.822	5.5	6.5	−0.03570	0.004703	0.00160
27549.30.....	3628.822	5.5	5.5	−0.01334	0.001757	0.04196
27549.30.....	3628.822	5.5	4.5	0.00532	−0.000700	0.12311
27549.30.....	3628.822	4.5	5.5	−0.03644	0.004800	0.00406
27549.30.....	3628.822	4.5	4.5	−0.01778	0.002343	0.04885
27549.30.....	3628.822	4.5	3.5	−0.00270	0.000356	0.08598
27549.30.....	3628.822	3.5	4.5	−0.03668	0.004832	0.00661

Notes.—Table 4 is published in its entirety in the electronic edition of the *Astrophysical Journal*. A portion is shown here for guidance regarding its form and content.

APPENDIX

TRANSITION DATA FOR *r*- AND *s*-PROCESS SURROGATES

Abundances of Eu and La are useful as surrogates for *r*- and *s*-process abundances in studies of Galactic halo stars (e.g., work on the rise of *s*-process by Simmerer et al. 2004). Modern transition probabilities based on a combination of radiative lifetimes from laser-induced fluorescence (LIF) measurements and branching fractions from an FTS for the important strong lines of Eu II and La II were reported by Lawler et al. (2001a, 2001c). These authors also collected the best available isotope shift (IS) and HFS data for the ground, low metastable, and resonance levels of Eu II and La II. They determined some of the missing IS and HFS data using FTS spectra.

A1. UPDATED La TRANSITION DATA

In Table 4 we present updated HFS patterns for 80 La II features, including 30 employed in this study. For all but four levels, these were computed using the best data compiled and/or measured by Lawler et al. (2001a): HFS constants for the upper levels at 22106.02 and 22537.30 cm^{-1} were updated using Li et al. (2001), and the upper levels at 24462.66 and 25973.37 cm^{-1} were updated using Limura et al. (2003). The component positions are referenced to the center-of-gravity (COG) wavenumbers and wavelengths. Transition wavenumbers were computed from NIST energy levels (Martin et al. 1978) and converted to air wavelengths using the standard index of air (Edlen 1953, 1966). Component strengths are normalized to sum to 1.

A2. UPDATED Eu TRANSITION DATA

During our earlier work on Eu II, it became apparent that the energy levels could be improved beyond that available from NIST (Martin et al. 1978). The NIST energy levels are from grating spectrometer measurements by Russell et al. (1941). Interferometric FTS accuracy (roughly ± 0.003 cm^{-1}) is at least an order of magnitude better than the accuracy of grating spectrometer measurements on photographic plates, particularly on lines with very wide ($\sim$1 cm^{-1}) IS and HFS patterns. Many of the critical Eu II lines to the

TABLE 5
Eu II Energy Levels

Energy Levels (cm^{-1})		
This Study[a]	NIST	*J*
0.000	0.00	4
1669.261	1669.21	3
9923.046	9923.00	2
10081.730	10081.65	3
10312.869	10312.82	4
10643.584	10643.48	5
11128.440	11128.22	6
23774.372	23774.28	3
24207.962	24207.86	4
26172.959	26172.83	5
26838.574	26838.50	4
27104.177	27104.07	3
27256.437	27256.35	2

[a] Accurate to 0.003 cm^{-1}.

TABLE 6
Isotopic Hyperfine Structure Patterns: ^{151}Eu and ^{153}Eu Solar System Mix

Wavenumber (cm^{-1})	λ (Å)	F_{upper}	F_{lower}	Component Position (cm^{-1})	Component Position (Å)	Strength
27104.177.....	3688.4183	5.5	6.5	−0.47314	0.064390	0.12395
27104.177.....	3688.4183	5.5	5.5	−0.13900	0.018916	0.01207
27104.177.....	3688.4183	5.5	4.5	0.14364	−0.019547	0.00057
27104.177.....	3688.4183	4.5	5.5	−0.10598	0.014423	0.09417
27104.177.....	3688.4183	4.5	4.5	0.17665	−0.024039	0.01840
27104.177.....	3688.4183	4.5	3.5	0.40782	−0.055498	0.00126
27104.177.....	3688.4183	3.5	4.5	0.19617	−0.026697	0.06956
27104.177.....	3688.4183	3.5	3.5	0.42735	−0.058155	0.01988
27104.177.....	3688.4183	3.5	2.5	0.60711	−0.082617	0.00163
27104.177.....	3688.4183	2.5	3.5	0.43788	−0.059588	0.04969

Notes.—Table 6 is published in its entirety in the electronic edition of the *Astrophysical Journal*. A portion is shown here for guidance regarding its form and content.

ground and first metastable levels have very wide structure. The wide structure is in part due to the large ($\sim$0.150 cm^{-1}) value of the IS from an unpaired 6*s* electron in the ground and lowest metastable levels.

Astrophysical data on halo stars from modern large telescopes have now reached the level of quality that isotopic abundances of Eu can be determined (e.g., Sneden et al. 2002). Evidence to date supports a uniform isotopic mix from all *r*-process events. The lines of Eu II connected to ground and lowest metastable levels are ideal for such studies.

In Table 5 we report FTS measurements of COG wavenumbers with a solar system isotopic mix of ^{151}Eu and ^{153}Eu (Rosman & Taylor 1998) for selected levels of Eu II. The procedure used in the Ho II work by Lawler et al. (2004) was followed. Internal standard Ar II and Ar I lines were used to calibrate the scale of four FTS spectra. The Ar II reference wavenumbers are from Learner & Thorne (1988) with a small correction by Whaling et al. (2002). The Ar I reference wavenumbers are from Whaling et al. (2002). Nonlinear least-squares fits of the complete line profiles, including all isotopic and hyperfine components, were performed to determine COG wavenumbers for 24 Eu II transitions. A global least-squares adjustment of the energy levels was performed using the redundant measured wavenumbers for the 24 transitions connected to the 13 levels of interest (12 excited levels, and the ground level defined as 0.00 cm^{-1}).

Since the publication of the earlier work on Eu II (Lawler et al. 2001c), requests have been made for lists of the complete hyperfine and IS patterns of the important lines of Eu II. While this information can be reconstructed from data in the earlier paper, some effort is required. Here we provide the complete isotopic and HFS structure patterns along with improved COG transition wavelengths (in air) for a solar system isotopic mix of ^{151}Eu and ^{153}Eu in Table 6. Energy levels from this work were combined with the best HFS constants from Table 4 and recommended line isotope shifts from Table 5 of Lawler et al. (2001c). Component positions are referenced to the COG values and component strengths are normalized to 1.000 for each line. The first half of the components listed for each line are from ^{151}Eu, and the second half are from ^{153}Eu.

REFERENCES

Alonso, A., Arribas, S., & Martínez-Roger, C. 1996, A&A, 313, 873
———. 1999, A&AS, 140, 261
Anders, E., & Grevesse, N. 1989, Geochim. Cosmochim. Acta, 53, 197
Andersen, T., Petersen, P., & Hauge, O. 1976, Sol. Phys., 49, 211
Aoki, W., Honda, S., Beers, T. C., & Sneden, C. 2003, ApJ, 586, 506
Aoki, W., Ryan, S. G., Norris, J. E., Beers, T. C., Ando, H., & Tsangarides, S. 2002, ApJ, 580, 1149
Argast, D., Samland, M., Thielemann, F.-K., & Qian, Y.-Z. 2004, A&A, 416, 997
Arlandini, C., Käppeler, F., Wisshak, K., Gallino, R., Lugaro, M., Busso, M., & Straniero, O. 1999, ApJ, 525, 886
Arnett, D., Truran, J. W., & Woosley, S. E. 1971, ApJ, 165, 87
Arnould, M., & Goriely, S. 2001, in ASP Conf. Ser. 245, Astrophysical Ages and Time Scales, ed. T. von Hippel, N. Manset, & C. Simpson (San Francisco: ASP), 252
Barklem, P. S., et al. 2005, A&A, 439, 129
Bergström, H., Lundberg, H., Persson, A., & Biémont, E. 1988, A&A, 192, 335
Bernath, P. F., Brazier, C. R., Olsen, T., Hailey, R., & Fernando, W. T. M. L. 1991, J. Mol. Spectrosc., 147, 16
Biémont, E., Garnir, H. P., Palmeri, P., Li, Z. S., & Svanberg, S. 2000, MNRAS, 312, 116
Biémont, E., Grevesse, N., Hannaford, P., & Lowe, R. M. 1981, ApJ, 248, 867
Biémont, E., Grevesse, N., Kwiatkowski, M., & Zimmermann, P. 1982, A&A, 108, 127
Biémont, E., Quinet, P., Dai, Z., Zhankui, J., Zhiguo, Z., Xu, H., & Svanberg, S. 2002, J. Phys. B, 35, 4743
Bisterzo, S., Gallino, R., Pignatari, M., Pompeia, L., Cunha, K., & Smith, V. 2004, Mem. Soc. Astron. Italiana, 75, 741
Burris, D. L., Pilachowski, C. A., Armandroff, T. A., Sneden, C., Cowan, J. J., & Roe, H. 2000, ApJ, 544, 302
Burstein, D., & Heiles, C. 1982, AJ, 87, 1165
Butcher, H. R. 1987, Nature, 328, 127
Cameron, A. G. W. 2003, ApJ, 587, 327
Cameron, A. G. W., Thielemann, F.-K., & Cowan, J. J. 1993, Phys. Rep., 227, 283
Carney, B. W., Latham, D. W., Stefanik, R. P., Laird, J. B., & Morse, J. A. 2003, AJ, 125, 293
Castelli, F., & Kurucz, R. L. 2003, in IAU Symp. 210, Modelling of Stellar Atmospheres, ed. N. E. Piskunov, W. W. Weiss, & D. F. Gray (San Francisco: ASP), 20
Cayrel, R., et al. 2001, Nature, 409, 691
Cohen, J. G., Christlieb, N., Qian, Y.-Z., & Wasserburg, G. J. 2003, ApJ, 588, 1082
Cowan, J. J., McWilliam, A., Sneden, C., & Burris, D. L. 1997, ApJ, 480, 246
Cowan, J. J., Pfeiffer, B., Kratz, K.-L., Thielemann, F.-K., Sneden, C., Burles, S., Tytler, D., & Beers, T. C. 1999, ApJ, 521, 194
Cowan, J. J., & Sneden, C. 2004, in Origin and Evolution of the Elements, ed. A. McWilliam & M. Rauch (Cambridge: Cambridge Univ. Press), 27
Cowan, J. J., & Thielemann, F.-K. 2004, Phys. Today, 57, 47
Cowan, J. J., et al. 2002, ApJ, 572, 861
———. 2005, ApJ, 627, 238
Cunningham, P. T., & Link, J. K. 1967, J. Opt. Soc. Am., 57, 1000
del Peloso, E. F., da Silva, L., & Arany-Prado, L. I. 2005, A&A, 434, 301
Den Hartog, E. A., Duquette, D. W., & Lawler, J. E. 1987, J. Opt. Soc. Am. B, 4, 48

Den Hartog, E. A., Lawler, J. E., Sneden, C., & Cowan, J. J. 2003, ApJS, 148, 543
Dinneen, T. P., Berrah Mansour, N., Kurtz, C., & Young, L. 1991, Phys. Rev. A, 43, 4824
Duquette, D. W., & Lawler, J. E. 1985, J. Opt. Soc. Am. B, 1, 1948
Edlen, B. 1953, J. Opt. Soc. Am., 43, 339
———. 1966, Metrologia, 2, 71
Erspamer, D., & North, P. 2003, A&A, 398, 1121
Fedchak, J. A., Den Hartog, E. A., Lawler, J. E., Palmeri, P., Quinet, P., & Biémont, E. 2000, ApJ, 542, 1109
Fitzpatrick, M. J., & Sneden, C. 1987, BAAS, 19, 1129
François, P., Spite, M., & Spite, F. 1993, A&A, 274, 821
Freiburghaus, C., Rosswog, S., & Thielemann, F.-K. 1999, ApJ, 525, L121
Fuhr, J. R., & Wiese, W. L. 2005, in NIST Atomic Transition Probability Tables, CRC Handbook of Chemistry and Physics, ed. D. R. Lide (Boca Raton: CRC), 78, 10
Fulbright, J. P. 2000, AJ, 120, 1841
Gilroy, K. K., Sneden, C., Pilachowski, C. A., & Cowan, J. J. 1988, ApJ, 327, 298
Gopka, V. F., Yushchenko, A. V., Mishenina, T. V., Kim, C., Musaev, F. A., & Bondar, A. V. 2004, Astron. Rep., 48, 577
Goswami, J. N., Marhas, K. K., Chaussidon, M., Gounelle, M., & Meyer, B. S. 2005, in ASP Conf. Ser. 341, Chondrites and the Protoplanetary Disk, ed. A. N. Krot, E. R. D. Scott, & B. Reipurth (San Francisco: ASP), 485
Gratton, R. G. 1989, A&A, 208, 171
Gratton, R. G., & Sneden, C. 1994, A&A, 287, 927
Grevesse, N., & Sauval, A. J. 1998, Space Sci. Rev., 85, 161
Griffin, R. F. 1968, A Photometric Atlas of the Spectrum of Arcturus, λλ3600–8825 Å (Cambridge: Cambridge Philos. Soc.)
Hannaford, P., Lowe, R. M., Biémont, E., & Grevesse, N. 1985, A&A, 143, 447
Hannaford, P., Lowe, R. M., Grevesse, N., Biémont, E., & Whaling, W. 1982, ApJ, 261, 736
Hansen, B. M. S., et al. 2004, ApJS, 155, 551
Herbig, G. H. 1975, ApJ, 196, 129
Hill, V., et al. 2002, A&A, 387, 560
Hoffman, R. D., Woosley, S. E., & Qian, Y.-Z. 1997, ApJ, 482, 951
Holweger, H., & Müller, E. A. 1974, Sol. Phys., 39, 19
Honda, S., Aoki, W., Kajino, T., Ando, H., Beers, T. C., Izumiura, H., Sadakane, K., & Takada-Hidai, M. 2004, ApJ, 607, 474
Ivans, I. I., Kraft, R. P., Sneden, C., Smith, G. H., Rich, M. R., & Shetrone, M. 2001, AJ, 122, 1438
Ivans, I. I., Sneden, C., Gallino, R., Cowan, J. J., & Preston, G. W. 2005, ApJ, 627, L145
Ivans, I. I., Sneden, C., James, C. R., Preston, G. W., Fulbright, J. P., Höflich, P. A., Carney, B. W., & Wheeler, J. C. 2003, ApJ, 592, 906
Ivans, I. I., Sneden, C., Kraft, R. P., Suntzeff, N. B., Smith, V. V., Langer, G. E., & Fulbright, J. P. 1999, AJ, 118, 1273
Ivarsson, S., Litzén, U., & Wahlgren, G. M. 2001, Phys. Scr., 64, 455
Ivarsson, S., et al. 2003, A&A, 409, 1141
Jimenez, R., Verde, L., Treu, T., & Stern, S. 2003, ApJ, 593, 622
Johnson, J. A., & Bolte, M. 2001, ApJ, 554, 888
———. 2004, ApJ, 605, 462
Johnson, J. A., Ivans, I. I., & Stetson, P. B. 2006, ApJ, 640, 801
Käppeler, F., Beer, H., & Wisshak, K. 1989, Rep. Prog. Phys., 52, 945
Klose, J. Z., Fuhr, J. R., & Wiese, W. L. 2002, J. Phys. Chem. Ref. Data, 31, 217
Kohri, K., Narayan, R., & Piran, T. 2005, ApJ, 629, 341
Kraft, R. P., & Ivans, I. I. 2003, PASP, 115, 143
Kratz, K.-L., Pfeiffer, B., Cowan, J. J., & Sneden, C. 2004, NewA Rev., 48, 105
Krauss, L. M., & Chaboyer, B. 2003, Science, 299, 65
Kurucz, R. L. 1998, in IAU Symp. 189, Fundamental Stellar Properties: The Interaction between Observation and Theory, ed. T. R. Bedding, A. J. Booth, & J. Davis (Dordrecht: Kluwer), 217
Kurucz, R. L., & Bell, B. 1995, Kurucz CD-ROM 23, Atomic Line Data (Cambridge: SAO)
Kurucz, R. L., Furenlid, I., Brault, J., & Testerman, L. 1984, Solar Flux Atlas from 296 to 1300 nm (Cambridge: Harvard Univ. Press)
Kwiatkowski, M., Zimmermann, P., Biémont, E., & Grevesse, N. 1982, A&A, 112, 337
———. 1984, A&A, 135, 59
Lawler, J. E., Bonvallet, G., & Sneden, C. 2001a, ApJ, 556, 452
Lawler, J. E., Den Hartog, E. A., Sneden, C., & Cowan, J. J. 2006, ApJS, 162, 227
Lawler, J. E., Sneden, C., & Cowan, J. J. 2004, ApJ, 604, 850
Lawler, J. E., Wickliffe, M. E., Cowley, C. R., & Sneden, C. 2001b, ApJS, 137, 341
Lawler, J. E., Wickliffe, M. E., den Hartog, E. A., & Sneden, C. 2001c, ApJ, 563, 1075
Learner, R. C. M., & Thorne, A. P. 1988, J. Opt. Soc. Am. B, 5, 2045
Li, G.-W., Zhang, X.-M., Lu, F.-Qu., Peng, X.-J., & Yang, F.-J. 2001, Japanese J. Appl. Phys., 40, 2508
Limura, H., et al. 2003, Phys. Rev. C, 68, 43281
Lodders, K. 2003, ApJ, 591, 1220
Martin, W. C., Zalubas, R., & Hagan, L. 1978, in Atomic Energy Levels: The Rare Earth Elements (NSRDS-NBS 60; Washington: GPO), 174
McWilliam, A. 1997, ARA&A, 35, 503
———. 1998, AJ, 115, 1640
McWilliam, A., Preston, G. W., Sneden, C., & Searle, L. 1995, AJ, 109, 2757
McWilliam, A., & Searle, L. 1999, Ap&SS, 265, 133
Meyer, B. S. 2005, in ASP Conf. Ser. 341, Chondrites and the Protoplanetary Disk, ed. A. N. Krot, E. R. D. Scott, & B. Reipurth (San Francisco: ASP), 515
Meyer, B. S., & Clayton, D. C. 2000, Space Sci. Rev., 92, 133
Migdalek, J., & Baylis, W. E. 1987, Canadian J. Phys., 65, 1612
Mishenina, T. V., & Kovtyukh, V. V. 2001, A&A, 370, 951
Mishenina, T. V., Kovtyukh, V. V., Soubiran, C., Travaglio, C., & Busso, M. 2002, A&A, 396, 189
Moore, C. E., Minnaert, M. G. J., & Houtgast, J. 1966, The Solar Spectrum 2934 Å to 8770 Å (NBS Monogr. 61; Washington: GPO)
Musaev, F., Galazutdinov, G., Sergeev, A., Karpov, N., & Pod'yachev, Y. 1999, Kinematics Phys. Select. Bodies, 15, 216
Nakamura, T., Umeda, H., Nomoto, K., Thielemann, F.-K., & Burrows, A. 1999, ApJ, 517, 193
Nilsson, A. E., Johansson, S., & Kurucz, R. L. 1991, Phys. Scr., 44, 226
Nilsson, A. E., Ljung, L., Lundberg, H., & Nielsen, K. E. 2006, A&A, 445, 1165
Nilsson, H., Zhang, Z. G., Lundberg, H., Johansson, S., & Nordström, B. 2002, A&A, 382, 368
O'Brian, T., Wickliffe, M., Lawler, J., Whaling, W., & Brault, J. 1991, J. Opt. Soc. Am. B, 8, 1185
O'Brien, S., Dababneh, S., Heil, M., Käppeler, F., Plag, R., Reifarth, R., Gallino, R., & Pignatari, M. 2003, Phys. Rev. C, 68, 035801
Otsuki, T., Tagoshi, H., Kajino, T., & Wanajo, S. 2000, ApJ, 533, 424
Pagel, B. E. J. 1989, in Evolutionary Phenomena in Galaxies, ed. J. E. Beckman & B. E. J. Pagel (Cambridge: Cambridge Univ. Press), 201
Palmeri, P., Quinet, P., Wyart, J.-F., & Biémont, E. 2000, Phys. Scr., 61, 323
Perryman, M. A. C., et al. 1997, The *Hipparcos* and Tycho Catalogues (ESA SP-1200; Noordjwik: ESA)
Persson, J. R. 1997, Z. Phys. D At. Mol. Clusters, 42, 259
Pfeiffer, B., Kratz, K.-L., & Thielemann, F.-K. 1997, Z. Phys. A Hadrons Nuclei, 357, 235
Pfeiffer, B., Ott, U., & Kratz, K.-L. 2001, Nucl. Phys. A, 688, 575
Plez, B., et al. 2004, A&A, 428, L9
Prochaska, J. X., & McWilliam, A. 2000, ApJ, 537, L57
Qian, Y.-Z. 2003, Prog. Part. Nucl. Phys., 50, 153
Qian, Y.-Z., & Wasserburg, G. J. 2000, Phys. Rep., 333, 77
———. 2001, ApJ, 552, L55
———. 2003, ApJ, 588, 1099
Ramírez, I., & Meléndez, J. 2005, ApJ, 626, 465
Rosman, K. J. R., & Taylor, P. D. P. 1998, J. Phys. Chem. Ref. Data, 27, 1275
Ross, J. E., & Aller, L. H. 1972, Sol. Phys., 25, 30
Rosswog, S., Liebendörfer, M., Thielemann, F.-K., Davies, M. B., Benz, W., & Piran, T. 1999, A&A, 341, 499
Russell, H. N., Albertson, W., & Davis, D. N. 1941, Phys. Rev., 60, 641
Ryan, S. G., Norris, J. E., & Beers, T. C. 1996, ApJ, 471, 254
Sasaqui, T., Kajino, T., & Balantekin, A. B. 2005, ApJ, 634, 534
Schatz, H., Toenjes, R., Kratz, K-L., Pfeiffer, B., Beers, T. C., Cowan, J. J., & Hill, V. 2002, ApJ, 579, 626
Schlegel, D. J., Finkbeiner, D. P., & Davis, M. 1998, ApJ, 500, 525
Schlegel, E. M. 2003, AJ, 125, 1426
Simmerer, J., Sneden, C., Cowan, J. J., Collier, J., Woolf, V. M., & Lawler, J. E. 2004, ApJ, 617, 1091
Simmerer, J., Sneden, C., Ivans, I. I., Kraft, R. P., Shetrone, M. D., & Smith, V. V. 2003, AJ, 125, 2018
Sneden, C. 1973, ApJ, 184, 839
Sneden, C., & Cowan, J. J. 2003, Science, 299, 70
Sneden, C., Cowan, J. J., Burris, D. L., & Truran, J. W. 1998, ApJ, 496, 235
Sneden, C., Cowan, J. J., Ivans, I. I., Fuller, G. M., Burles, S., Beers, T. C., & Lawler, J. E. 2000a, ApJ, 533, L139
Sneden, C., Cowan, J. J., Lawler, J. E., Burles, S., Beers, T. C., & Fuller, G. M. 2002, ApJ, 566, L25
Sneden, C., Johnson, J., Kraft, R. P., Smith, G. H., Cowan, J. J., & Bolte, M. S. 2000b, ApJ, 536, L85
Sneden, C., Kraft, R. P., Guhathakurta, P., Peterson, R. C., & Fulbright, J. P. 2004, AJ, 127, 2162
Sneden, C., Kraft, R. P., Prosser, C. F., & Langer, G. E. 1991, AJ, 102, 2001
Sneden, C., McWilliam, A., Preston, G. W., Cowan, J. J., Burris, D. L., & Armosky, B. J. 1996, ApJ, 467, 819
Sneden, C., Pilachowski, C. A., & VandenBerg, D. A. 1986, ApJ, 311, 826
Sneden, C., et al. 2003, ApJ, 591, 936

Soubiran, C., Katz, D., & Cayrel, R. 1998, A&AS, 133, 221
Spergel, D. N., et al. 2003, ApJS, 148, 175
Tegmark, M., et al. 2004, Phys. Rev. D, 69, 103501
Terasawa, M., Sumiyoshi, K., Yamada, S., Suzuki, H., & Kajino, T. 2002, ApJ, 578, L137
Thielemann, F.-K., et al. 2001, in Proc. 27th Int. Cosmic Ray Conf. (Hamburg), 52
Travaglio, C., Gallino, R., Arnone, R., Cowan, J. J., Jordan, F., & Sneden, C. 2004, ApJ, 601, 864
Truran, J. W., Cowan, J. J., & Fields, B. D. 2001, Nucl. Phys. A, 688, 330
Truran, J. W., Cowan, J. J., Pilachowski, C. A., & Sneden, C. 2002, PASP, 114, 1293
Tull, R. G., MacQueen, P. J., Sneden, C., & Lambert, D. L. 1995, PASP, 107, 251
Venn, K. A., Irwin, M., Shetrone, M. D., Tout, C. A., Hill, V., & Tolstoy, E. 2004, AJ, 128, 1177
Villemoes, P., Arnesen, A., Heijkenskjöld, F., Kastberg, A., & Larsson, M. O. 1992, Phys. Scr., 46, 45
Voges, W., et al. 1999, A&A, 349, 389
Vogt, S. S., et al. 1994, Proc. SPIE, 2198, 362
Wallerstein, G., Greenstein, J. L., Parker, R., Helfer, H. L., & Aller, L. H. 1963, ApJ, 137, 280
Wanajo, S., Itoh, N., Ishimaru, Y., Nozawa, S., & Beers, T. C. 2002, ApJ, 577, 853
Wännström, A., Gough, D. S., & Hannaford, P. 1994, Z. Phys. D At. Mol. Clusters, 29, 39
Wasserburg, G. J., Busso, M., & Gallino, R. 1996, ApJ, 466, L109
Wasserburg, G. J., Busso, M., Gallino, R., & Nollett, K. M. 2006, Nucl. Phys. A, in press (astro-ph/0602551)
Wasserburg, G. J., & Qian, Y.-Z. 2000, ApJ, 529, L21
Westin, J., Sneden, C., Gustafsson, B., & Cowan, J. J. 2000, ApJ, 530, 783
Whaling, W., Anderson, W. H. C., Carle, M. T., Brault, J. W., & Zarem, H. A. 2002, J. Res. NIST, 107, 149
Whaling, W., & Brault, J. W. 1988, Phys. Scr., 38, 707
Wheeler, J. C., Cowan, J. J., & Hillebrandt, W. 1998, ApJ, 493, L101
Wickliffe, M. E., & Lawler, J. E. 1997, J. Opt. Soc. Am. B, 14, 737
Wickliffe, M. E., Lawler, J. E., & Nave, G. 2000, J. Quant. Spectrosc. Radiat. Transfer, 66, 363
Wickliffe, M. E., Salih, S., & Lawler, J. E. 1994, J. Quant. Spectrosc. Radiat. Transfer, 51, 545
Woosley, S. E., & Hoffman, R. D. 1992, ApJ, 395, 202
Xu, H., Jiang, Z., Zhang, Z., Dai, Z., Svanberg, S., Quinet, P., & Biémont, E. 2003, J. Phys. B, 36, 1771
Yushchenko, A., et al. 2002, J. Korean Astron. Soc., 35, 209
———. 2005, A&A, 430, 255